Original Article

MOLECULAR METABOLISM

# A Neural basis for Octanoic acid regulation of energy balance

Vanessa R. Haynes [1,2,7], Natalie J. Michael [2,6,7], Marco van den Top [5], Fei-Yue Zhao [5], Russell D. Brown [2], David De Souza [4], Garron T. Dodd [1], David Spanswick [2,3,5,**], Matthew J. Watt [1,8,*]

## ABSTRACT

**Objectives:** Nutrient sensing by hypothalamic neurons is critical for the regulation of food intake and energy expenditure. We aimed to identify long- and medium-chain fatty acid species transported into the brain, their effects on energy balance, and the mechanisms by which they regulate activity of hypothalamic neurons.

**Methods:** Simultaneous blood and cerebrospinal fluid (CSF) sampling was undertaken in rats and metabolic analyses using radiolabeled fatty acid tracers were performed on mice. Electrophysiological recording techniques were used to investigate signaling mechanisms underlying fatty acid-induced changes in activity of pro-opiomelanocortin (POMC) neurons.

**Results:** Medium-chain fatty acid (MCFA) octanoic acid (C8:0), unlike long-chain fatty acids, was rapidly transported into the hypothalamus of mice and almost exclusively oxidized, causing rapid, transient reductions in food intake and increased energy expenditure. Octanoic acid differentially regulates the excitability of POMC neurons, activating these neurons directly via GPR40 and inducing inhibition via an indirect non-synaptic, purine, and adenosine receptor-dependent mechanism.

**Conclusions:** MCFA octanoic acid is a central signaling nutrient that targets POMC neurons via distinct direct and indirect signal transduction pathways to instigate changes in energy status. These results could explain the beneficial health effects that accompany MCFA consumption.


**Keywords** Fatty acid metabolism; Pro-opiomelanocortin neuron; Food intake; Energy expenditure; Electrophysiology; Cerebrospinal fluid

## 1. INTRODUCTION

The integration of hormone and nutrient signals in the central nervous system is essential for the appropriate regulation of body weight homeostasis [1]. Disturbances in the detection of or response to metabolic signals form the cornerstone of metabolic diseases such as obesity and type 2 diabetes [2,3]. Of the central neural pathways regulating energy homeostasis, the melanocortin system is one of the most important [4,5]. Consisting of two functionally antagonistic neuronal populations located within the arcuate nucleus (ARC) of the hypothalamus, orexigenic neuropeptide-Y/agouti-related peptide (NPY/AgRP) and anorexigenic pro-opiomelanocortin (POMC) neurons coordinate counter-regulatory responses to oppose alterations in energy balance. Both NPY and POMC neurons express leptin and insulin receptors and alter their activity in response to these and other circulating nutrients and hormones such as glucose, ghrelin, and glucagon-like peptide-1 (GLP-1), which reflect metabolic status [6–9]. The regulation of POMC neurons has been shown to specifically influence both food intake and energy expenditure to attenuate weight gain in response to short-term energy surfeit [10,11].

Long-chain fatty acids (LCFAs) are generally thought of as signals of nutrient surplus [12] and have been shown to regulate the activity of neurons within numerous hypothalamic nuclei [13–15]. LCFAs are capable of acting centrally to modulate food intake and body weight [16], effects that have been attributed to intracellular accumulation of LCFA-CoA rather than their oxidation [12,15]. Despite these reported effects, the fatty acids that can readily cross the blood–brain barrier and physiologically relevant concentrations of fatty acids achieved in the cerebrospinal fluid (CSF) remain relatively unknown. In addition, the role of medium-chain fatty acids (MCFAs) and effects of fatty acids on functionally identified neurons within the arcuate nucleus is largely unknown and may be important in the context of satiation and energy balance.

[1]Department of Physiology, Faculty of Medicine, Dentistry and Health Sciences, University of Melbourne, Melbourne, 3010, VIC, Australia [2]Metabolic Disease, Obesity and Diabetes Program, Biomedicine Discovery Institute and the Department of Physiology, Monash University, Clayton, 3800, VIC, Australia [3]Warwick Medical School, University of Warwick, Coventry, CV4 7AL, UK [4]Metabolomics Australia, Bio21 Institute, University of Melbourne, Parkville, 3010, VIC, Australia [5]NeuroSolutions Ltd, Coventry, UK [6]Center for Hypothalamic Research, Department of Internal Medicine, UT Southwestern Medical Center, Dallas, TX, 75390, USA

[7] These authors contributed equally to this work.
[8] Lead contact.

*Corresponding author. Department of Physiology, University of Melbourne, Melbourne, Victoria, 3010, Australia.Tel. +613 8344 8663. E-mail: matt.watt@unimelb.edu.au (M.J. Watt).

**Corresponding author. Metabolic Disease, Obesity and Diabetes Program, Biomedicine Discovery Institute, Department of Physiology, Monash University, Clayton, 3800, VIC, Australia.Tel. +61 3 9902 4307. E-mail: david.spanswick@monash.edu (D. Spanswick).

Received June 20, 2019 • Revision received December 11, 2019 • Accepted January 3, 2020 • Available online 9 January 2020

https://doi.org/10.1016/j.molmet.2020.01.002

 

**Abbreviations**

| | |
|---|---|
| AgRP | agouti-related peptide |
| ANOVA | analysis of variance |
| ARC | arcuate nucleus |
| aCSF | artificial CSF |
| KATP | ATP-sensitive potassium channels |
| CNS | central nervous system |
| CSF | cerebrospinal fluid |
| IV | current voltage |
| FAT/CD36 | fatty acid translocase |
| FFA | free fatty acid |
| FFA1/GPR40 | free fatty acid receptor 1 |
| GLP-1 | glucagon-like peptide-1 |
| HFD | high-fat diet |
| LCFA | long-chain fatty acid |
| LCT | long-chain triglyceride |
| MCFA | medium-chain fatty acid |
| MCT | medium-chain triglyceride |
| NPY | neuropeptide-Y |
| PSC | peripheral sensor controller |
| POMC | pro-opiomelanocortin |
| RER | respiratory exchange ratio |
| TTX | tetrodotoxin |
| VLCFA | very-long-chain fatty acid |

Unlike LCFAs, which must first traverse the lymphatic system, MCFAs are transported via the portal venous system and are rapidly absorbed into the circulation and tissues. MCFAs promote satiation and increase energy expenditure, and diets enriched with MCFA reduce adiposity compared with diets high in LCFAs [17–22]. Recent studies have shown that POMC neurons express free fatty acid receptor 1 (FFA1/GPR40) [23,24], suggesting a potential role of MCFAs to directly regulate the electrical activity of ARC POMC neurons, a process that may explain the effects of MCFAs on food intake and energy expenditure. Herein, we describe the unappreciated role of MCFA octanoic acid (C8:0) in regulating POMC-mediated control of food intake and energy expenditure and describe direct and indirect signaling pathways by which this MCFA regulates electrical excitability of these neurons.

## 2. MATERIALS AND METHODS

### 2.1. Rat studies

Experiments using rats were conducted according to the Animals (Scientific Procedures) Act, 1986 (UK Government Home Office). Male Wistar Han rats were maintained on a standard rodent chow diet (7.4% total digestible energy from lipids and 11.9 mJ/kg total digestible energy; RM1P, Special Diet Services, Essex, UK). At 6 weeks old, the rats either continued on the chow diet or were changed to a high-fat diet (HFD; 42.0% total digestible energy from lipids and 20.4 MJ/kg total; 829,100, Special Diet Services, Essex, UK) for a period of 20 weeks. The experiments were conducted at 26 weeks.

#### 2.1.1. Intravenous glucose tolerance test and cerebrospinal fluid collection

The methodology for this part of the study was described in detail previously (49). D-glucose (D1610, Fisher Scientific) was dissolved in distilled water to a concentration of 250 mg/mL. A glucose bolus (500 mg/kg) was IV injected through the jugular vein cannula. CSF and blood samples were collected before (0 min) and at 5, 10, 20, 30, 60, 90, and 120 min following the glucose injection (see below).

The rats were anesthetized with isoflurane for induction (5%/95% volume, Isorrane, AHN3640, Baxter Healthcare) followed by sodium pentobarbitone 50 mg/kg via intraperitoneal injection for maintenance. Each animal was placed in a supine position, and a cannula (Portex Intravenous Cannula Pink base #3F, 1.0 mm OD) filled with normal saline (0.9%) was inserted into the right side jugular vein. The tubing was fixed in place by two ligations using 4/0 stitch silk. Each rat was placed in a temperature-controlled recovery chamber for 90 min before the first blood and CSF sampling to avoid aerosol anesthetic-induced hyperglycemia. The anesthesia level was monitored throughout the procedures and maintained by regular top-ups of pentobarbitone through the jugular vein cannula.

Each animal's head was manually held for CSF sample collection. The neck was shaved, a small incision was made above the obex, and the muscle was carefully pulled apart with a small stretcher to expose the atlantooccipital membrane. Approximately 20 μL of CSF was drawn from the cisterna magna using a 25 gauge needle attached to a 1 mL syringe. The sample was placed in a 500 μL tube, snap-frozen using dry ice, and stored at −80 °C for later lipidomic and metabolomic analysis (Section 3.1). For blood sample collection, a cut was made on each rat's tail-tip. A small drop of blood sample (8–10 μL) was examined with an Accu-Chek Glucose Meter System and 100 μL of blood was collected into microtubes containing anticoagulant ethylenediamine-tetra-acetic acid (EDTA; 450474CN, Greiner Bio-One). The blood sample was shaken, snap-frozen on dry ice, and stored at −80 °C for later analysis.

#### 2.1.2. Analysis of cerebrospinal fluid and blood free fatty acids by GC–MS

CSF and blood samples from the 0 time point of the GTT (prior to injection of the glucose bolus) were used for metabolomic analysis. A 20 μL aliquot of whole blood or CSF was combined with 60 μL methanol and 20 μL chloroform containing 500 μM $^{13}C_2$-myristic acid as an internal standard. The samples were incubated at room temperature for 15 min, then centrifuged at 16,000×*g* for 5 min at 4 °C to pellet precipitated proteins. A 50 μl aliquot of the supernatant was transferred to a fresh tube, to which 20 μl acidified (0.1 M hydrogen chloride) Milli-Q $H_2O$ was added to facilitate biphasic partitioning and push the fatty acids into the chloroform phase. A total of 50 μl of chloroform was added to enable quantitative recovery of the lipid phase. Then 45 μl of the chloroform phase was transferred to a glass vial insert and evaporated to dryness in vacuo. The dried samples were derivatized by the addition of 30 μl N,O-bis(trimethylsilyl)trifluoroacetamide with trimethylchlorosilane (BSTFA + 1% TMCS; Pierce Technologies) at 37 °C for 2 h with constant mixing. Fatty acid standards were prepared in the range of 1.56–200 μM and derivatized via the previously described method.

The samples were analyzed using an Agilent 7890 Gas Chromatograph coupled to a 5975C Mass Selective Detector. A 1 μl aliquot sample was injected into the GC inlet set at 250 °C, and chromatographic separation was achieved using an SGE BPX70 column (60 m × 0.25 mm i.d. X 0.25 μM film thickness). The GC oven ramp was started at 70 °C and maintained for 1 min before ramping at 40 °C/min to 150 °C and then 4 °C/min to 250 °C and maintained for a further 6 min. Compounds were

 

fragmented via electron impact ionization and detected in the selected ion monitoring mode, and characteristic fragments including the molecular ions were used for each fatty acid.
Resultant chromatograms were analyzed using Agilent's MassHunter Quantitative Analysis software. Areas were integrated for target ions for each fatty acid in all of the samples and standards. Standard curves were plotted and used only when the $R^2$ value was greater than 0.9. Concentrations were calculated from the standard curves, followed by correction for dilution.

### 2.2. Mouse studies

Mouse experimental procedures were approved by the Monash Animal Research Platform Animal Ethics Committee, Monash University (MARP-1/2014/008) and conformed to National Health and Medical Research Council (Australia) guidelines regarding the care and use of experimental animals. Mice were fed a chow diet (9% total digestible energy from lipids, 12.8 MJ/kg; Barastoc Irradiated Mice Cubes, Ridley AgriProducts) and water ad libitum. Mice aged 6 weeks either continued on the chow diet or were changed to a HFD (43.0% total digestible energy from lipids, 19.0 MJ/kg; SF04-001, Specialty Feeds). The experiments were conducted when the mice were 12 weeks old.

#### 2.2.1. In vivo hypothalamic fatty acid metabolism: intracerebral ventricular administration

To measure hypothalamic fatty acid (FA) metabolism in vivo, FAs were administered via intracerebral cannulation of the left ventricle. A lateral ventricle guide cannula (Plastics One, C315GS-4-SPC, 26 gauge, 4 mm pedestal, cut at a depth of 2 mm below the skull) was placed −0.3 mm anteroposterior and +1.0 mm lateral to the bregma in 12-week-old male C57Bl/6J mice using sterile techniques under general anesthesia induced and maintained by isoflurane inhalation (1.5%; Isorrane, Baxter Healthcare, AHN3640). The cannula support plate was attached to the skull and the incision site was closed. A dummy cannula was inserted to temporarily seal the guide cannula. Three days later, the conscious mice were restrained, and the dummy cannula was removed. An internal cannula connected to a 10 μL syringe was inserted into the guide cannula, and 2 μL of 1 mCi/mL of [1−$^{14}$C]-oleic acid (Perkin Elmer, NEC317250UC), [1−$^{14}$C]-palmitic acid (Perkin Elmer, NEC075H250UC), or [1−$^{14}$C]-octanoic acid (American Radiolabeled Chemicals Inc., ARC0149) was injected over 30 s. Thirty min later, the mice were anesthetized via isoflurane inhalation, decapitated, and the brain removed. A scalpel was used to isolate the mediobasal hypothalamus, defined caudally by the mammillary bodies, rostrally by the optic chiasm, laterally by the optic tract, and superiorly by the apex of the hypothalamic third ventricle. A section of the cortex/hippocampus/thalamus (CHT) brain region was also collected. The liver, mixed quadriceps skeletal muscle, and gonadal WAT were then collected. The tissues were weighed, washed twice with cold PBS, transferred to 12 × 75 mm glass test tubes containing chloroform:methanol 2:1 (v:v), and homogenized. The expired $^{14}CO_2$ was not collected from the mice, so the complete FA oxidation was not assessed. Incomplete FA oxidation, as indicated by the production of acid soluble metabolites, and FA storage as glycerides was measured as described in 2.3.1. The values were normalized to the wet tissue mass.

#### 2.2.2. In vivo hypothalamic fatty acid metabolism: carotid artery administration

Male 12-week-old C57Bl/6J mice were anesthetized as previously described and the right carotid artery was cannulated with PE50 polyethylene tubing (Plastics One). From time point 0, 200 μL of 0.9% sodium chloride with 0.1% BSA and 2 μCi/mL [1−$^{14}$C]-oleic acid, [1−$^{14}$C]-palmitic acid, or [1−$^{14}$C]-octanoic acid was infused over 5 min at a rate of 40 μL/min. The mice remained under anesthesia for a further 10 min. Tail blood was collected at baseline and every 2 min throughout the infusion using 5 μL disposable pipettes (Microcaps, Drummond Scientific). The mice were euthanized via decapitation without regaining consciousness and the brain was removed. A scalpel was used to isolate the mediobasal hypothalamus and samples of the CHT brain region, liver, skeletal muscle, and WAT as described. As explained in Section 2.2.1, a modified Folch lipid extraction [25] was performed and FA metabolism was measured.

#### 2.2.3. In vivo hypothalamic fatty acid metabolism: oral gavage administration

Male 12-week-old C57Bl/6J mice were fasted for 2 h to ensure no food was present in the stomach. The mice were restrained and 100 μL of water with 1% BSA, 100 μM oleic acid (250 μCi/mL [1−$^{14}$C]-oleic acid), or octanoic acid (250 μCi/mL [1−$^{14}$C]-octanoic acid) was administered via a feeding needle (22 gauge, 1 inch straight needle with a 1.25 mm ball; Braintree Scientific, N-PK002). The mice were returned to their cage after the gavage. Tail blood was collected using disposable 5 μL pipettes at baseline and every 7 min thereafter. At 60 min, tissues were collected and FA metabolism was assessed as described in Section 2.2.1.

#### 2.2.4. Assessment of food intake

Male C57Bl/6J mice were fed a standard rodent chow (9% total digestible energy from lipids, 12.8 MJ/kg; Barastoc Irradiated Mice Cubes, Ridley AgriProducts). The mice were individually housed in cages with a perimeter-mounted food hopper and spill tray attached to a BioDAQ (Research Diets Inc.) peripheral sensor controller (PSC). The PSC measured the weight once per second, and changes in the stable weight were recorded along with the date and time, thus providing second-by-second food intake data.
Following a 3-day acclimation period, a randomized cross-over trial was conducted. At day 0, the mice were weighed and then fasted from 1400 to 1600 h. Between 1600 and 1630 h, the mice were given an oral gavage with 175 μl water, a long-chain fatty acid triglyceride (LCT; glyceryl trioleate, 92,860, Sigma−Aldrich; 177 μl and 5.5 kJ, accounting for ∼10% of daily caloric intake), or a medium-chain fatty acid triglyceride (MCT; glyceryl trioctanoate, SC-215091, Santa Cruz Biotechnology; 173 μl and 5.5 kJ, accounting for ∼10% of daily caloric intake). Food intake data was collected uninterrupted for 46 h. The mice were not handled during this period. At 1400 h on day 2, the mice were weighed, fasted from 1400 to 1600 h, and given an oral gavage of the next solution. Thus, each mouse received the 3 gavage solutions in a random order 48 h apart. At the end of the study, the mice were weighed and culled. A BioDAQ DataViewer (Research Diets Inc.) was used to compile the data.

#### 2.2.5. Indirect gas exchange calorimetry analysis

Male 12-week-old C57Bl/6J mice were housed individually in indirect gas exchange calorimetry chambers (CaloSys, TSE Systems). A randomized cross-over trial was conducted as previously described in Section 2.2.4. Following triglyceride or water gavage, oxygen consumption ($VO_2$) and carbon dioxide production ($VCO_2$) were measured for 48 h. The respiratory exchange rate (RER) was calculated as $VCO_2$/$VO_2$. The energy expenditure was calculated from $VO_2$ and RER using Weir constants [26] and normalized to the body mass.

#### 2.2.6. Functional immunohistochemistry

The mice were fasted from 1400 to 1600 h then given an oral gavage of either water, LCT, or MCT as described in Section 2.2.4. At 90 min

 

post-gavage, the mice were anesthetized and perfused transcardially with heparinized saline (10,000 units/l heparin in 0.9% (w/v) NaCl) followed by 4% (w/v) paraformaldehyde in phosphate buffer (0.1 M, pH 7.4). Their brains were post-fixed overnight and maintained for four days in 30% (w/v) sucrose in 0.1 M phosphate buffer to cryoprotect the tissue before freezing on dry ice. Then 30 mm sections (120 mm apart) were cut in the coronal plane throughout the entire rostral-caudal extent of the hypothalamus. For immunostaining, the sections were incubated at room temperature for 1 h in blocking buffer (0.1 M phosphate buffer, 0.2% (v/v) Triton X-100, and 10% (v/v) normal goat serum) and then incubated overnight at 4 °C in rabbit c-Fos antibody (1:4000, sc-52, Santa Cruz, CA, USA) or guinea pig anti-α-MSH (1/1000; AS597, Antibody Australia) in 1% (v/v) blocking buffer. For both c-Fos and α-MSH immunohistochemistry, the sections were incubated for 2 h at room temperature with goat anti-rabbit or goat anti-guinea pig Alexa-Fluor-568-conjugated secondary antibody in 5% (v/v) blocking buffer. The sections were mounted with Mowiol 4–88 mounting media and visualized using an Olympus BX 3000 microscope. To determine the fluorometric integrated density of α-MSH staining in the PVH, a region of interest was first drawn around the PVH using ImageJ software. All of the images underwent skeletonization using a consistent threshold setting and the integrated density was quantified using ImageJ software. Brightness and contrast were uniformly adjusted to aid visualization.

#### 2.2.7. Electrophysiology

For the electrophysiology component of the study, 6–16 week POMC eGFP mice were used as previously described [6]. The mice were fasted overnight (~16.5 h) to replicate conditions in which plasma FFA are normally increased. On the day of the experiment, the animals were terminally anesthetized using isoflurane and the brain harvested. Coronal 250 μM thick slices of brain containing the hypothalamus were cut using a vibrating blade microtome (Leica VT1000 S). The slices were cut in cold (<4°) artificial CSF (aCSF) containing (in mM): 127 NaCl, 1.2 $KH_2PO_4$, 1.9 KCl, 26.0 $NaHCO_3$, 0.5–1 D-glucose, 9–9.5 mannitol, 2.4 $CaCl_2$, and 1.3 $MgCl_2$ equilibrated with 95% $O_2$ and 5% $CO_2$ pH 7.4 The slices were immediately warmed at 34° for 20 min before returning to room temperature prior to recording.

The intracellular solution contained (in mM) 140 K-gluconate, 10 KCl, 10 HEPES, 1 EGTA, and 1 ATP; the pH and osmolarity were adjusted with KOH and sucrose, respectively. POMC eGFP-positive neurons were visualized and recorded using a combination of epifluorescence and differential interference contrast (IR-DIC) optics. Whole-cell patch clamp recordings were made using an Axopatch 1D amplifier with pipettes with resistances ranging between 5 and 12 MΩ when filled with intracellular solution. Data were acquired on a PC running pClamp data acquisition software Clampex 9.2 (Axon Instruments), filtered, and digitally stored for later offline analysis. Analysis of the electrophysiological data was carried out using Clampfit.

Octanoic acid (Sigma) was prepared as a concentrated stock (100 mM) in 100% ethanol. On the day of the experiments, the octanoic acid was diluted to the required concentration (4–40 μM) in aCSF and applied to the slice chamber via superfusion of a specified volume (20 mL). Appropriate vehicle controls were also used. Antagonists were similarly prepared and aliquoted as concentrated stocks in distilled water or DMSO and diluted in aCSF on the day of the experiments to the required concentrations. The antagonists were applied by superfusion for at least 10 min or following the application of sufficient volume to saturate the recording chamber at the required concentration prior to testing the octanoic acid. The presence of antagonist was maintained throughout exposure to the octanoic acid. The following antagonists were used: GPR40 antagonist DC260126, adenosine A1 receptor antagonist DPCPX, A2a receptor antagonist istradefylline, A2b receptor antagonist PSB603 (Tocris), and A3 receptor antagonist MRS1523 (Santa Cruz Biotechnology). Tetrodotoxin (TTX, Abcam) was prepared as a concentrated stock (1 mM) and stored frozen until use when it was diluted in aCSF to the required concentration. Carbenoxolone (Sigma) was prepared fresh on the day of the experiment, dissolved directly in aCSF, and applied to the slices for at least 40 min prior to testing octanoic acid.

### 2.3. Cell culture studies

N29/4 cells were purchased from CELLutions Biosystems (CLU115, Cedarlane Laboratory, Hornby, ON, Canada). The immortalized line was created from mouse embryonic day 15, 17, and 18 hypothalamic neuron primary cultures and immortalized by retroviral transfer of SV40 T-Ag. The cells were grown in 25 mM glucose Dulbecco's Modified Eagle Medium GlutaMAX (DMEM; Gibco-Invitrogen, #10569) supplemented with 10% fetal bovine serum (FBS; Gibco-Invitrogen, #16000) and 1% penicillin-streptomycin (pen/strep; Gibco-Invitrogen, #15140) at 37 °C, with 5.0% carbon dioxide ($CO_2$) incubation. The experiments were conducted on the cells at 100% confluence between passages 2 and 16.

Dulbecco's Modified Eagle Medium (DMEM) containing 5.56 mM glucose was supplemented with 2% fatty acid-free BSA, 1% pen/strep, and either 0 or 1.0 mM oleic acid (C18:1; Sigma–Aldrich, 01008), palmitic acid (C16:0; Sigma–Aldrich, P-0500), and octanoic acid (C8:0; Sigma–Aldrich, C2875). The medium was filter sterilized (0.20 μm) and applied to neurons for 4 or 18 h as specified. Cells were washed with 1X phosphate buffered saline (PBS; Invitrogen, #14040133) after treatments. Lysates were collected in the PBS, transferred to glass test tubes with chloroform:methanol 2:1 (v:v), vigorously mixed, and then spun at 1000×*g* at 4 °C for 10 min. The organic phase was transferred to a glass tube, dried under nitrogen gas at 40 °C, and reconstituted in 10 μL of ethanol. The triglyceride content was measured biochemically (Roche, Basel, Switzerland, #11730711).

#### 2.3.1. Fatty acid metabolism

The base medium consisted of DMEM, with or without 5.56 mM glucose, and 2% BSA. Thereafter, 0.5 mM oleic acid, palmitic acid, or octanoic acid and 0.5 μCi/mL [1–$^{14}$C]-oleic acid, [1–$^{14}$C]-palmitic acid, or [1–$^{14}$C]-octanoic acid was added and incubated for 1 h at 37 °C to allow conjugation of the FA to the BSA. The cells were incubated in the respective treatment media for 4 h at 37 °C. The medium was removed and added to 1 mL of 1 M perchloric acid in a 25 mL glass vial. The glass vial also contained a 1.7 mL Eppendorf tube that housed a 500 μL Eppendorf tube containing 300 μL benzethonium hydroxide. The glass tube was sealed immediately to capture the $^{14}CO_2$ contained in the culture medium and radioactivity was determined by liquid scintillation counting (Beckman Coulter Scintillation Counter LS6500). The released $^{14}CO_2$ represented complete fatty acid oxidation and was normalized to the total protein.

The cells were washed twice with PBS and lysed in 0.1% Triton X-100 (Sigma–Aldrich, #9002-93-1) in PBS. The lysates were transferred to glass test tubes with chloroform:methanol 2:1 (v:v), vigorously mixed, and then spun at 1000×*g* at 4 °C for 10 min. The aqueous phase was transferred to a scintillation tube with 5 mL scintillation cocktail and counted to assess $^{14}$C labeled acid soluble metabolites, which represented the incomplete fatty acid oxidation. The organic phase was transferred to a 12 × 75 mm glass tube, dried under nitrogen gas at 40 °C, and reconstituted in 50 μL chloroform:methanol (2:1)

 

containing ~3 mg of lipid standards (dipalmitate, Sigma–Aldrich, D2636 and tripalmitate, Sigma–Aldrich, TS5888). The samples were spotted onto 250 μm glass-backed silica gel plates and the lipids were separated by thin layer chromatography in a resolving solution containing heptane:isopropyl ether:acetic acid (60:40:3). The plates were air-dried and sprayed with 2′,7′-dichlorofluorescein dye (0.02% w/v in ethanol). The lipid bands were visualized under UV light and then scraped into scintillation vials for assessment of radioactivity. All of the values were normalized to the total cellular protein.

### 2.4. Statistical analysis

All of the statistical analyses were conducted using the statistical package GraphPad Prism version 6.0e (GraphPad Software, San Diego, CA, USA). $P < 0.05$ was considered statistically significant. Data were reported as mean ± standard error of the mean (SEM). Metabolomics and FA metabolism were analyzed using Student's unpaired t-test (two-tailed) or a one-way analysis of variance (ANOVA). Food intake, body weight, energy expenditure, RER, and activity level data were analyzed by two-way ANOVA with the Bonferroni post hoc test. Patch clamp electrophysiology was analyzed by paired t-tests or one-way ANOVA. Parametric statistics were used when the data displayed a Gaussian distribution in all of the conditions, and non-parametric statistics were used when this assumption was not met.

## 3. RESULTS

### 3.1. Free fatty acid composition of the cerebrospinal fluid

While fatty acids are established as regulators of food intake [16], the precise molecular species mediating this effect are unresolved. Accordingly, we used liquid chromatography tandem mass spectrometry to investigate the composition of fatty acids of various chain lengths and degrees of saturation in the CSF. We also examined the free fatty acid (FFA) composition of blood that was simultaneously obtained from the same rats, which were fed a chow or high-fat diet (HFD). The rats fed a HFD had increased body weight and mildly impaired glucose tolerance compared with the chow-fed rats (Figure S1). Total FFA levels were 2.5-fold higher in the blood compared with the CSF and did not differ between the rats fed a chow or HFD (Figure 1A). Individual FFAs are reported in Table S1. It is noteworthy that plasma FFA levels and FFA profiles are often similar between chow and HFD-fed rodents, particularly in the fasted state [27], which aligns with human studies reporting similar plasma FFA levels [28] and FFA profiles [29] between lean and obese individuals.

In the blood, 41% of the total FFAs were saturated, 16% were monounsaturated, and 42% were polyunsaturated. Strikingly, the CSF was composed almost exclusively of saturated FFA (89%), with negligible concentrations of mono- and polyunsaturated FFA (4% and 7%, respectively) (Figure 1B). The distribution of the fatty acids by chain length was also different between the blood and CSF. The blood was predominantly composed of LCFA, which accounted for 96% of the FFAs, with lower concentrations of very-long-chain fatty acids (VLCFAs, 3%) and MCFAs (1%) (Figure 1C). LCFAs accounted for 94% of all of the FFAs in the CSF and VLCFAs were barely detectable (Figure 1C). The major LCFAs present in the CSF were palmitic acid (C16:0, 51%) and stearic acid (C18:0, 27%) (Figure 1E). Oleic acid (C18:1) was at low concentrations in the CSF, accounting for only 1% of the total CSF FFAs (Figure 1E). This is notable because oleic acid was previously used to study FFA effects on food intake, energy expenditure, and central nervous system (CNS) control of glucose metabolism [16,30]. MCFAs constituted 4% of all of the CSF FFAs (Figure 1C), with octanoic acid ($CH_3(CH_2)_6COOH$, C8:0) accounting for 78% of the MCFAs (Figure 1D). Notably, the concentration of octanoic acid was close to equimolar in the blood and CSF, suggesting bidirectional movement across the blood–brain barrier and/or a potential role in regulating CNS function.

### 3.2. Octanoic acid, but not long-chain fatty acids, easily traverse between the circulation and CSF and are predominantly oxidized

To elucidate the potential role of specific fatty acids in CNS control of food intake and energy homeostasis, we compared the metabolic fates of the LCFAs (oleic acid and palmitic acid) and the MCFA octanoic acid in hypothalamic-derived N24 neurons. The neurons were capable of transporting fatty acids across the plasma membrane, oxidizing fatty acids, and storing fatty acids as glycerides (Figure 2A). The neurons preferentially stored rather than oxidized the LCFAs, as reflected by an oxidation to storage ratio of 1:5 for oleic acid (C18:1) and 1:3 for palmitic acid (C16:0) (Figure 2B). In contrast, the neurons oxidized rather than stored octanoic acid (ratio of 5:1). Consistent with these results, prolonged exposure to LCFAs, but not octanoic acid, resulted in storage of intracellular triglyceride in the neurons (Figure 2C).

To determine the in vivo relevance of these observations, fatty acid metabolism was assessed in the hypothalamus of the conscious mice. The FFAs were administered directly to the CSF via the lateral ventricle and the metabolic fate of the FAs was assessed 30 min thereafter. Octanoic acid oxidation was 90-fold higher than the oleic and palmitic acid despite being delivered at equimolar concentrations (Figure 2D). Similar to the results observed in the cultured neurons, the LCFAs were preferentially stored as glycerides (1:5 and 1:3 oxidation to storage ratio for the oleic acid and palmitic acid, respectively), while the octanoic acid was almost exclusively oxidized rather than stored (33:1 oxidation to storage ratio) (Figure 2E). Notably, the octanoic acid rapidly traversed from the CNS into the peripheral circulation where it was oxidized by tissues including the liver, skeletal muscle, and white adipose tissue (Figure S2). Radiolabeled oleic and palmitic acid showed limited movement from the CSF to the plasma (Figures S2C-E), demonstrating that octanoic acid readily crosses the blood–brain barrier, whereas LCFA transport is negligible.

While the intracerebroventricular administration of FFA tests the capacity for FFA metabolism in the hypothalamus, this route of administration bears no physiological relevance. Therefore, radiolabeled FFAs were administered via the right carotid artery and the FFA metabolism was assessed. Infusion of the FFAs was successful as shown by increased radioactivity in the blood of the mice (Figure 2F). Oleic and palmitic acid uptake into the hypothalamus was negligible (Figure 2G), and the majority of the LCFAs remained in the circulation and were metabolized by the liver (Figure S2H). In contrast, the octanoic acid was readily taken up and oxidized in the hypothalamus, with an oxidation to storage ratio of 31:1 (Figure 2G,H).

To determine the metabolic fate of FFAs administered directly to the gut, conscious mice received radiolabeled oleic acid or octanoic acid via oral gavage (Figure 2I). There were negligible levels of oleic acid detected in the hypothalamus 1 h after administration (Figure 2J) and the oleic acid was readily metabolized by the liver (Figure S2M). In contrast, the octanoic acid rapidly crossed from the gut (Figure 2I, within 7 min) and was almost exclusively oxidized rather than stored by the hypothalamus (Figure 2K). Altogether, these experiments demonstrate that the parenchyma of the hypothalamus (including neurons) is capable of fatty acid transport, oxidation, and storage. Importantly, octanoic acid readily crosses from the circulation into the hypothalamus and is predominately oxidized, while there is limited movement into, or oxidation of, LCFAs by the hypothalamus.

 

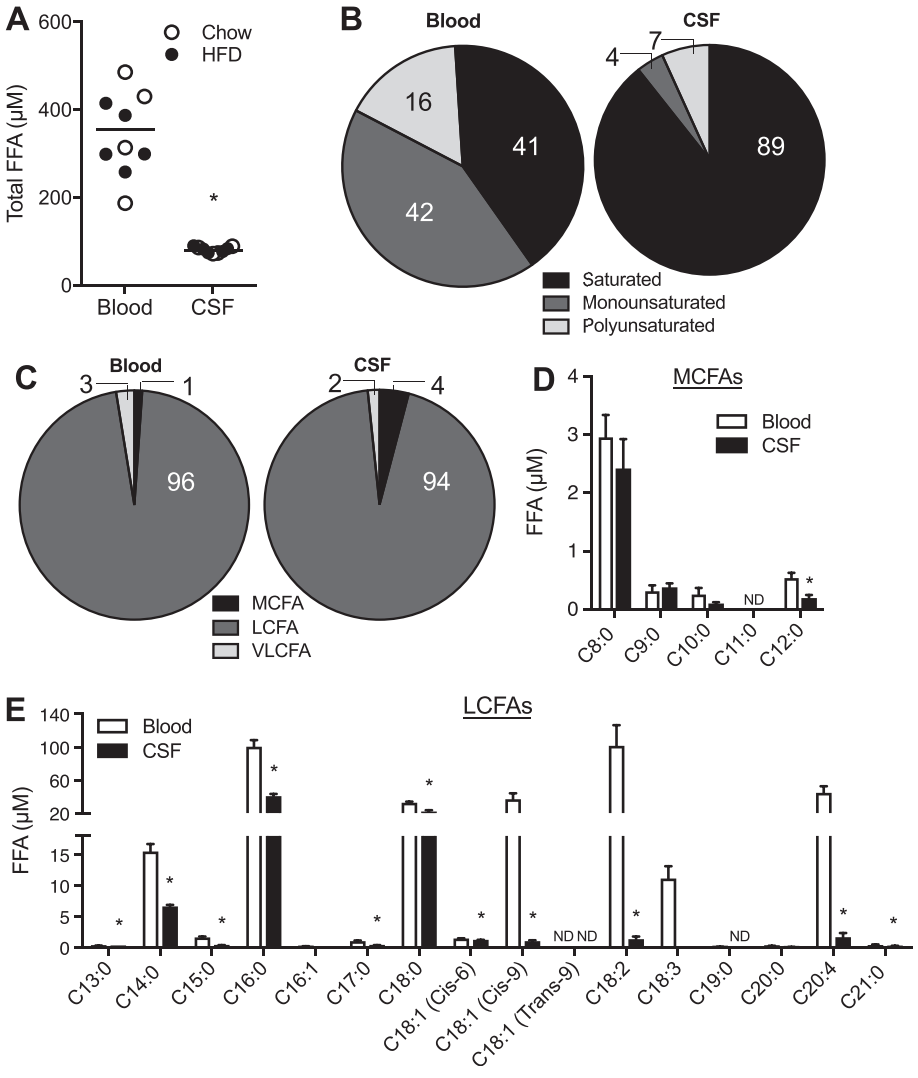


**Figure 1:** Free fatty acid composition of cerebrospinal fluid and blood. (A) Total FFA levels in the blood and CSF in rats fed chow (n = 4) or HFD (n = 5). (B) Proportion of FFA in blood and CSF by saturation. (C) Proportion of FFA in blood and CSF by chain length. (D) Concentration of medium-chain fatty acids (MCFA) in the blood and CSF. (E) Concentration of individual long-chain fatty acids (LCFA) in the blood and CSF. For panels B–E, data are mean ± SEM, n = 4 chow. *P < 0.05 between groups. Statistical analysis by two-tailed paired t-test.

### 3.3. Trioctanoic acid, but not trioleic acid, regulates energy homeostasis in lean mice

Given that octanoic acid rapidly traverses from the gut to the CSF and is rapidly oxidized (Figure 2I–J), we surmised that octanoic acid is an important signaling lipid in the CNS that may regulate energy homeostasis. To test this hypothesis, lean mice were given an oral gavage of water, trioleic acid (long-chain triglyceride, LCT), or trioctanoic acid (medium-chain triglyceride, MCT). The caloric content of the triglyceride loads was equal to 10% of each mouse's predetermined daily calorie intake and was administered just prior to the main eating period (1600 h) to determine whether the fatty acids promoted an anorexic response. MCT administration reduced food intake by 53% compared with water and 41% compared with the LCT in the first 8 h after gavage (Figure 3A). Even when the initial caloric load was considered, food intake remained markedly suppressed by MCT administration (Figure 3B). LCT administration reduced total food intake by 20% in the first 8 h after gavage; however, there was no difference between LCT and water gavage when the energy content of the LCT gavage was calculated into the total caloric load (Figure 3B). There were no differences in caloric intake between the groups between 8 and 48 h post-gavage, suggesting that there was no "rebound" increase in food intake in the MCT-treated mice (Figure S3).

The reduced food intake following MCT gavage was preceded by an increase in oxygen consumption compared with water and LCT gavage (Figure 3C–D). Unlike the prolonged effect on food intake, there was no difference in oxygen consumption between treatments from 4 to 8 h post-gavage. The MCT-mediated increase in oxygen consumption was accompanied by a small but significant increase in physical activity (Figure 3E–F), and no such changes were observed in the LCT-treated mice. There was no difference in whole-body RER between the treatment groups (Figure 3G–H). Together, these data demonstrate that mice respond to MCT by rapidly and transiently reducing their food intake and increasing their energy expenditure.

 

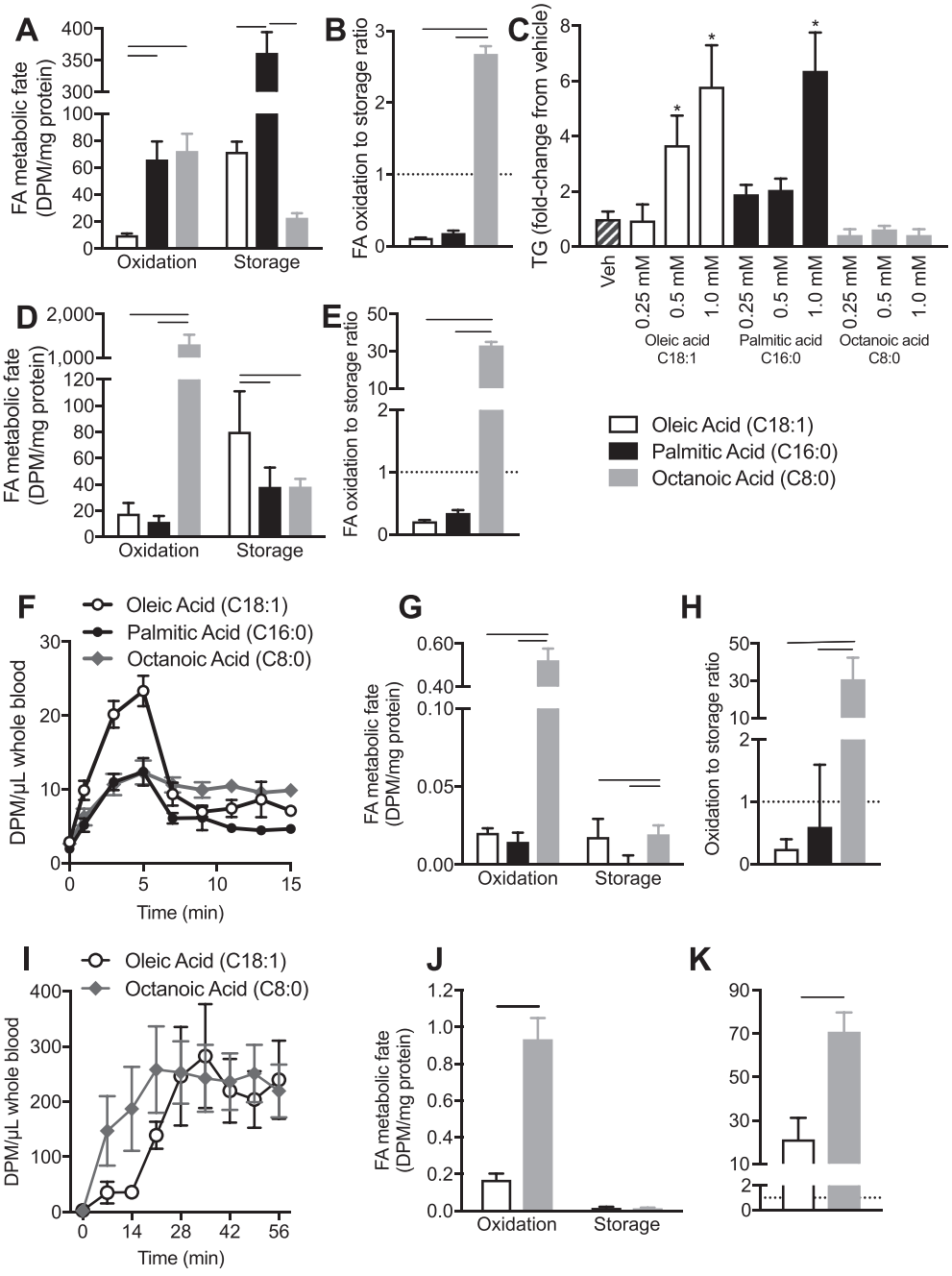


**Figure 2:** Metabolism of fatty acids in hypothalamic neurons and the parenchyma of the hypothalamus in vivo. **(A–C)** Metabolism of oleic acid, palmitic acid, and octanoic acid in cultured N24 hypothalamic neurons. **(A)** Fatty acid oxidation and storage in triglycerides (TG). **(B)** Oxidation to storage ratio of the various fatty acids. Data are mean ± SEM. n = 5 oleic acid, n = 6 palmitic acid, and n = 6 octanoic acid from three independent experiments. **(C)** TG accumulation in cultured N24 hypothalamic neurons after 18 h exposure to fatty acids. *P < 0.05 compared to vehicle, n = 3–6. **(D–E)** Fatty acid metabolism in the hypothalamus 30 min after intracerebral ventricular (ICV) administration of fatty acids in mice. **(D)** Fatty acid oxidation and storage in triglycerides. **(E)** Oxidation to storage ratio of the various fatty acids. n = 5 oleic acid, n = 5 palmitic acid, and n = 8 octanoic acid. **(F–H)** Fatty acid metabolism in the hypothalamus 15 min after administration of fatty acids via the carotid artery in mice. **(F)** $^{14}C$ levels in whole blood during (0–5 min) and after (5–15 min) arterial infusion of $^{14}C$ fatty acids. **(G)** Fatty acid oxidation and storage in triglycerides. **(H)** Oxidation to storage ratio of the various fatty acids. n = 8 oleic acid, n = 4 palmitic acid, and n = 6 octanoic acid. **(I–K)** Fatty acid metabolism in the hypothalamus 60 min after oral gavage of fatty acids in mice. **(I)** $^{14}C$ levels in whole blood before and after oral administration of $^{14}C$ fatty acids. **(J)** Fatty acid oxidation and storage in triglycerides. **(K)** Oxidation to storage ratio of the various fatty acids. n = 4 oleic acid, and n = 3 octanoic acid. For all of the panels, p < 0.05 indicated by lines adjoining bars. Statistical analysis by one-way analysis of variance with Bonferroni post hoc tests for the data in panels A, B, D, E, G, H, J, and K.

 

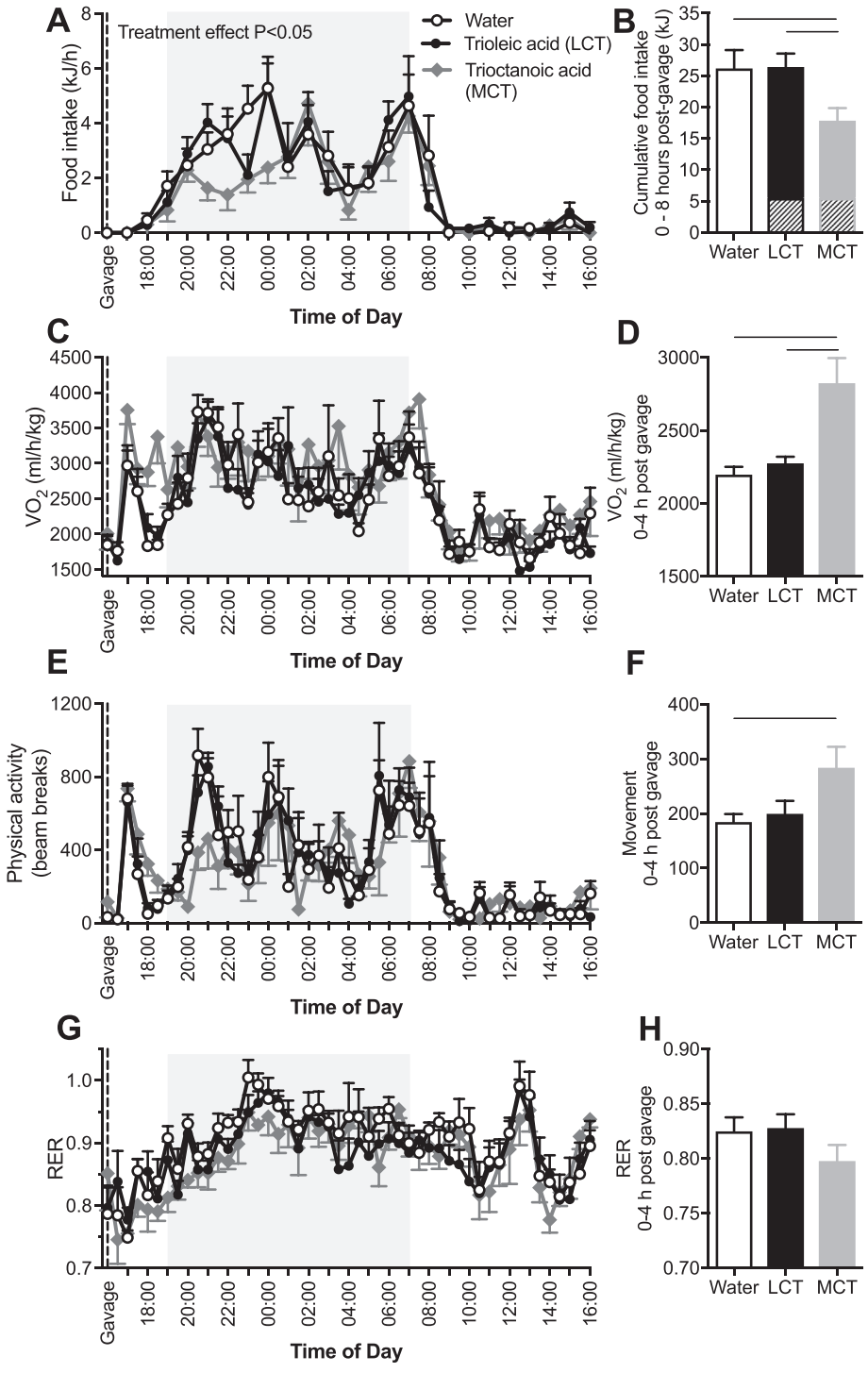


**Figure 3:** Octanoic acid, but not long-chain fatty acids, rapidly and transiently reduced food intake and increase energy expenditure. Water, trioleate (long-chain triglyceride, LCT), or trioctanoic acid (medium-chain triglyceride, MCT) was administered to mice by oral gavage immediately prior to the evening feeding period (1600 h) in a randomized cross-over design. **(A)** Food intake monitored over 24 h and **(B)** during the 8 h after oral gavage. Hatched portion of the bars represents caloric content of the oral gavage triglyceride. n = 10 mice per group. **(C)** Oxygen consumption ($VO_2$) monitored over 24 h and **(D)** during the 4 h after oral gavage. n = 6 mice per group. **(E)** Physical activity monitored over 24 h and **(F)** during the 4 h after oral gavage. n = 6 mice per group. **(G)** The respiratory exchange ratio (RER) monitored over 24 h and **(H)** during the 4 h after oral gavage. n = 6 mice per group. Data are mean ± SEM. For all of the panels, $p < 0.05$ indicated by lines adjoining bars. Statistical analysis by two-way analysis of variance for data in panels A, C, E, and G. Statistical analysis by one-way analysis of variance for data in panels B, D, F, and H.

 

### 3.4. Trioctanoic acid, but not trioleic acid, enhanced melanocortin output in the hypothalamus of lean mice

Our results indicate that oral MCT administration enters the brain CSF, attenuates food intake, and increases energy expenditure. A critical central regulator of energy homeostasis is the melanocortin system within the hypothalamus [31]. The melanocortin system, comprised in part by POMC neurons in the ARC, has the capacity to attenuate food intake and increase energy expenditure via the release of α-MSH from POMC neurons innervating the PVH (Figure 4A) [32]. We postulated that MCT effects on energy homeostasis may be through modulation of this hypothalamic melanocortin circuitry. To determine the capacity of MCT to increase melanocortin output within the hypothalamus, we stained for α-MSH in the PVH of the C57BL/6J mice administered water, MCT, or LCT. We found that α-MSH staining in the PVH was increased in the MCT- but not LCT-treated mice (Figure 4B–C). Next, to determine whether the enhanced melanocortin response to MCT is of functional relevance in vivo, we measured the activation of neurons in the PVH of the mice administered either water, LCT, or MCT. Administration of MCT, but not LCT, increased c-Fos staining (a surrogate marker of neuronal activation) in the PVH (Figure 4D–E). Taken together, MCT enhanced α-MSH and increased neuronal activity within the PVH, which is consistent with a role of MCT in regulating the hypothalamic melanocortin output known to regulate energy homeostasis [33–35].

### 3.5. Electrophysiological characterization of the effects of octanoic acid on ARC POMC neurons

The anorexigenic effects of octanoic acid, increased melanocortin output, and increased energy expenditure were consistent with a potential role in directly regulating the electrical activity of ARC POMC neurons. Accordingly, POMC neurons in brain slices containing the ARC were visualized and recorded. POMC neurons included in this study had a resting membrane potential of $-47.6 \pm 0.7$ mV ($n = 95$) and input resistance of $1263 \pm 54$ MΩ ($n = 100$). Most of the POMC cells were spontaneously active, with an average firing rate of $2.14 \pm 0.35$ Hz ($n = 60$). The electrophysiological properties of the POMC neurons in the present study are consistent with those reported previously [6,36,37].

Octanoic acid differentially regulated POMC neuronal excitability, inducing inhibition and membrane hyperpolarization in 31.8% ($n = 34$), excitation and membrane depolarization in 27.1% ($n = 29$), and biphasic responses in 7.5% ($n = 8$) of the POMC neurons, the latter characterized by excitation preceding membrane hyperpolarization and inhibition to levels beyond control resting potentials. The remaining 36 (33.6%) of the POMC neurons were insensitive to octanoic acid (Figure 5A).

Octanoic acid-induced excitation (Figure 5B) was characterized by membrane depolarization of $5.0 \pm 0.6$ mV (from $-47.4 \pm 0.9$ mV to $-42.4 \pm 0.7$ mV in the presence of octanoic acid; $n = 34$, $p < 0.001$) associated with an increase in firing frequency of $1.13 \pm 0.24$ Hz (baseline: $0.68 \pm 0.18$ Hz; octanoic acid: $1.81 \pm 0.35$Hz; $n = 34$, $p < 0.001$) and an increase in neuronal input resistance amounting to $396 \pm 105$ MΩ (baseline, $1431 \pm 181$ MΩ; octanoic acid, $1800 \pm 216$ MΩ; $n = 8$, $p < 0.01$; Figure 5E–G). The increase in input resistance was consistent with the closure of ion channels and a decrease in whole-cell conductance. The voltage–current (VI) relationship confirmed octanoic acid-induced excitation associated with an increase in neuronal input resistance and a reversal potential of $-86 \pm 3.2$ mV ($n = 7$; Figure 5C,D), close to the reversal potential for potassium ions under our recording conditions. These data indicate octanoic acid-induced excitation via closure of one or more resting potassium conductances.

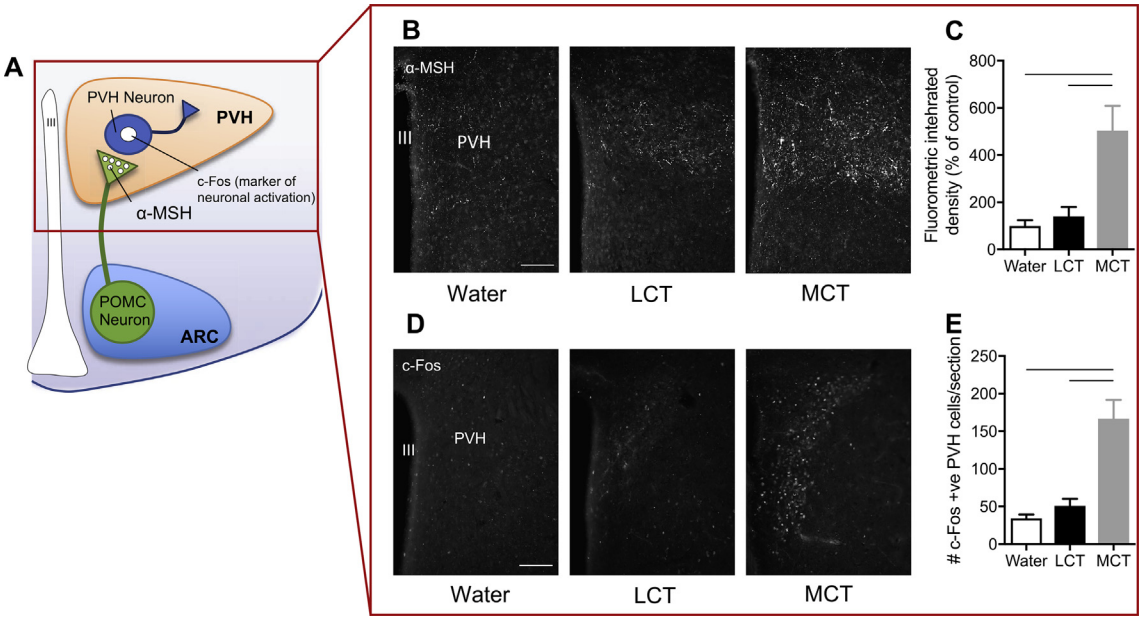


**Figure 4:** Medium-chain triglyceride but not long-chain triglyceride stimulates POMC neuronal melanocortin output to the paraventricular nucleus of the hypothalamus. **(A)** Schematic depicting the melanocortin output from POMC neurons to the paraventricular nucleus of the hypothalamus (PVH). α-MSH release from POMC neurons terminating in the PVH activates post synaptic PVH neurons to suppress food intake. The 9-week-old C57Bl/6J male mice were administered (orally) water, trioleate (long-chain triglyceride, LCT), or trioctanoic acid (medium-chain triglyceride, MCT). Then 90 min later, brains were fixed with paraformaldehyde and processed for PVH. **(B–C)** α-MSH and **(D–E)** c-Fos immunoreactivity. Scale bar = 200 μm. Data are mean ± SEM. For all of the panels, $p < 0.05$ indicated by lines adjoining bars. Statistical analysis by one-way analysis of variance for data in panels C and E. $n = 5$ mice per group. Abbreviations: III, third ventricle; α-MSH, alpha melanocyte-stimulating hormone; ARC, arcuate nucleus of the hypothalamus; PVH, paraventricular nucleus of the hypothalamus.

 

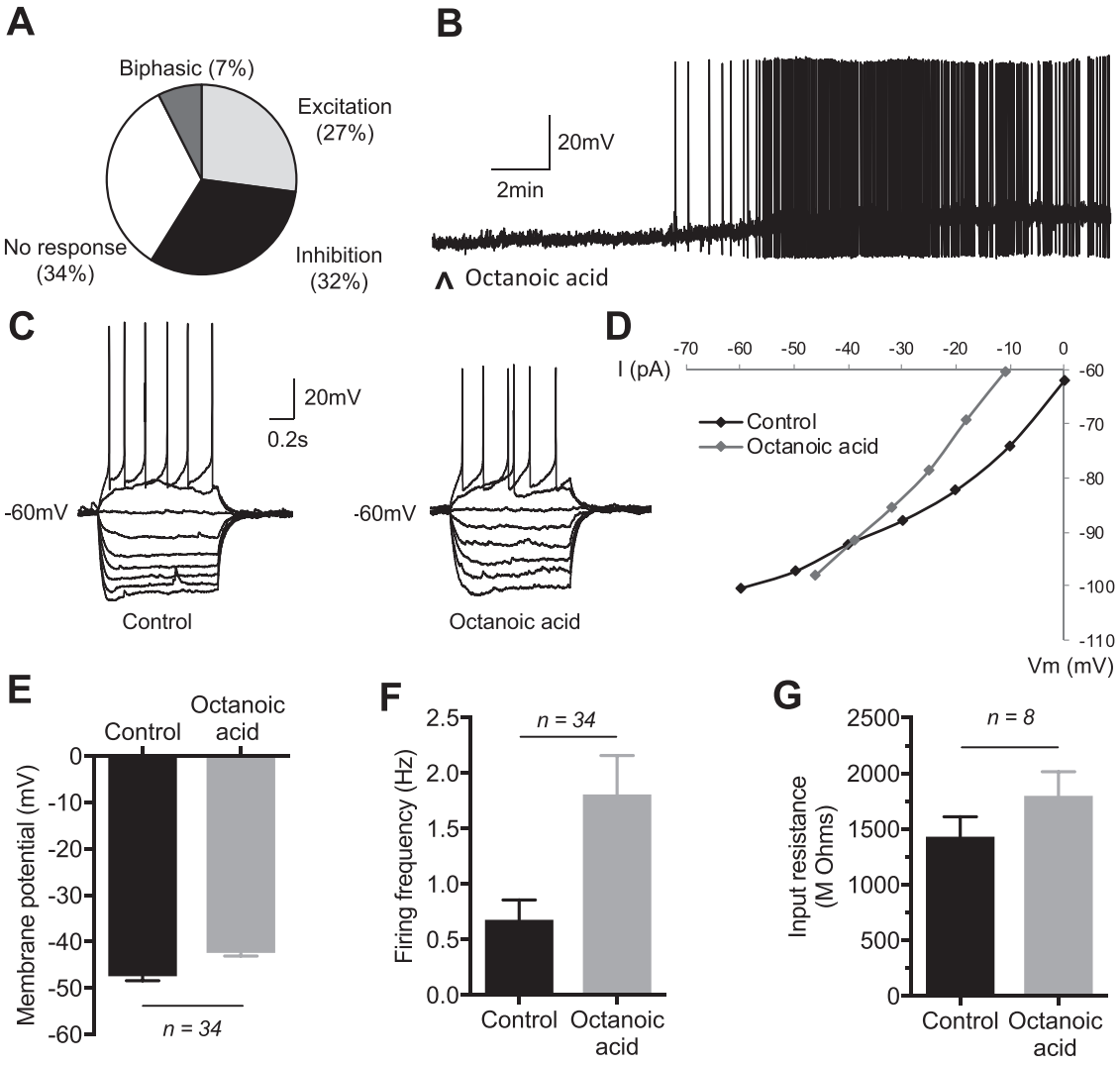


**Figure 5:** Electrophysiological effects of octanoic acid on ARC POMC neurons: octanoic acid-induced excitation. **(A)** Overview pie chart showing the relative numbers of ARC POMC neurons characterized by their response to octanoic acid. n = 107 cells; 34 inhibited, 29 excited, 8 showed a biphasic response (inhibition and excitation), and 36 were insensitive to octanoic acid. **(B)** Representative example of a whole-cell current clamp recording from an ARC POMC neuron showing octanoic acid-induced membrane depolarization and increased firing rate. **(C)** Current–voltage (IV) relationships generated by injection of a linearly increasing series of negative and positive current pulses (not shown) recorded in the absence (control) and during octanoic acid-induced depolarization in an ARC POMC neuron. **(D)** Plot of IV relationships shown in C. Note the increase in the slope of the plot in the presence of octanoic acid, indicating block or inhibition of a resting conductance. Note also the linear IV relationship in octanoic acid compared to control at negative membrane potentials and point of intersection more negative than −90 mV, indicating octanoic acid-induced depolarization via block of inwardly rectifying potassium conductance. **(E)** Mean change in membrane potential of octanoic acid excited POMC neurons (n = 34; $p < 0.001$). **(F)** Mean change in firing frequency of octanoic acid excited POMC neurons (n = 34; $p < 0.001$). **(G)** Mean change in input resistance of octanoic acid excited POMC neurons (n = 8; $p < 0.01$). Note in B ^ indicates 20 ml of 40 μM octanoic acid applied by superfusion. Data are mean ± SEM. For panels E, F, and G, $p < 0.05$ indicated by lines adjoining bars. Statistical analysis by paired two-tailed t-tests.

Octanoic acid-induced inhibition of the POMC neurons was characterized by membrane hyperpolarization of 4.4 ± 0.6 mV (from −45.3 ± 0.9 mV to −49.6 ± 1.1 mV; n = 40, $p < 0.001$) associated with a decrease in the spontaneous action potential firing rate by 0.82 ± 0.16 Hz (baseline: 1.06 ± 0.22 Hz; octanoic acid: 0.24 ± 0.09 Hz; n = 42, $p < 0.001$) and a reduction in the neuronal input resistance amounting to 478 ± 119 MΩ (baseline: 1521 ± 220 MΩ; octanoic acid: 1043 ± 153 MΩ; n = 14, $p < 0.01$) (Figure 6A, D, E, and F). The VI relationship revealed octanoic acid-induced inhibition associated with a reversal potential of −70 mV ± 4.4 mV (n = 9; range −57 to −100 mV), midway between the predicted reversal potentials for potassium and chloride ions (Figure 6B,C). Taken together, these data indicate octanoic acid-induced inhibition via opening of the potassium and/or chloride ion channels.

### 3.6. Octanoic acid-induced activation of POMC neurons is mediated via GPR40 receptors

Having established the ionic mechanisms underlying octanoic acid-induced changes in POMC neuronal excitability, we further explored aspects of the signal transduction pathway. Octanoic acid-induced excitation of POMC neurons (n = 11) was blocked in the presence of the free fatty acid receptor FFA1 (GPR40) antagonist DC260126 in the majority of the POMC neurons tested (10/11: Figure 7A). Furthermore, blocking of the fatty acid-induced excitation with DC260126 uncovered an octanoic acid-induced inhibition in 6 of these

 

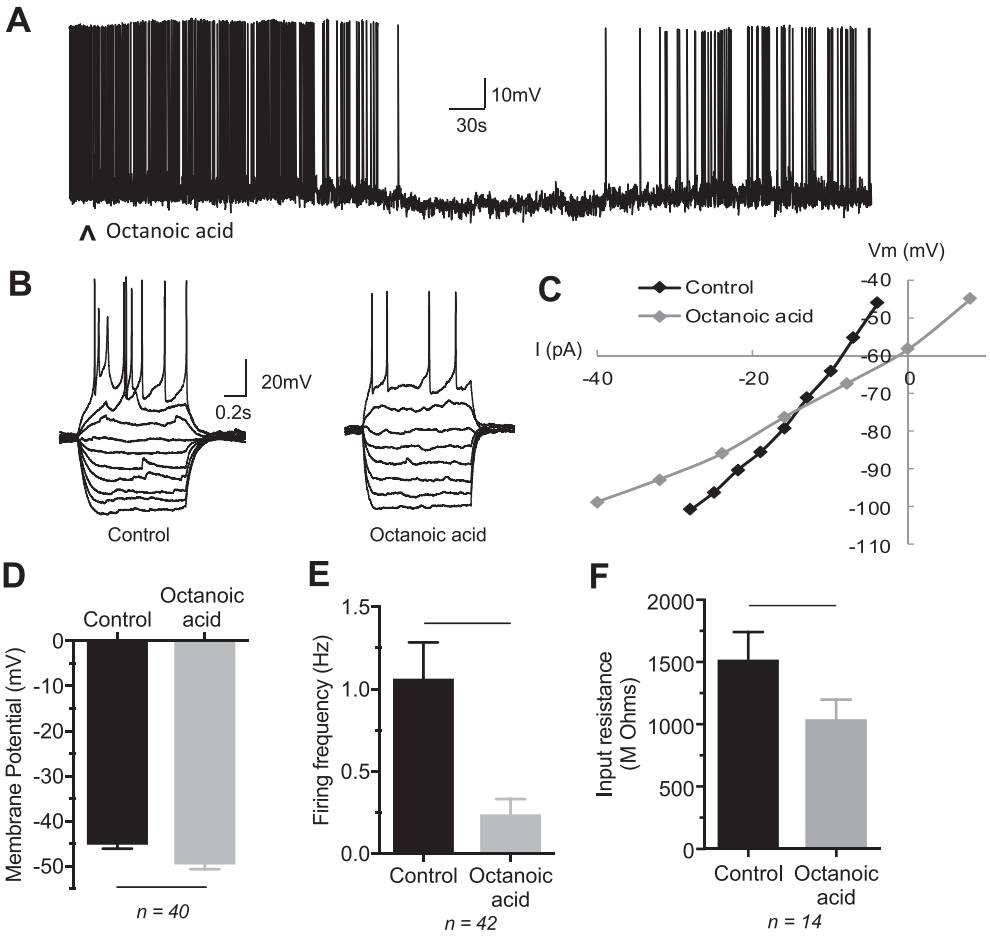


**Figure 6:** Electrophysiological effects of octanoic acid on ARC POMC neurons: octanoic acid-induced inhibition. **(A)** Representative example of a whole-cell current clamp recording from an ARC POMC neuron showing octanoic acid-induced membrane hyperpolarization and inhibition of firing. **(B)** IV relationships of an ARC POMC neuron before (control) and during octanoic acid-induced inhibition of activity in a POMC neuron. **(C)** Plot of IV relationships shown in B. Note the decrease in the slope of the plot associated with octanoic acid-induced inhibition, indicating activation of a conductance. **(D)** Mean change in membrane potential of octanoic acid-induced inhibition of POMC neurons ($n = 40$; $p < 0.001$). **(E)** Mean change in firing rate of octanoic acid inhibited POMC neurons ($n = 42$; $p < 0.001$). **(F)** Mean change in input resistance of octanoic acid inhibited POMC neurons ($n = 14$; $p < 0.01$). Note in A ^ indicates 20 mL of 40 μM octanoic acid applied by superfusion. Data are mean ± SEM. For panels D, E, and F, $p < 0.05$ indicated by lines adjoining bars. Statistical analysis by paired t-tests.

neurons. In a further 7 POMC neurons, octanoic acid alone induced inhibition, whereas subsequent exposure to DC260126 failed to block this effect. Overall, in 13 of the 18 neurons exposed to this GPR40 antagonist, octanoic acid-induced inhibition persisted, characterized by membrane hyperpolarization associated with a reduction or cessation in spontaneous action potential firing (Figure 7B,C). These data suggest a pivotal role of GPR40 in mediating octanoic acid-induced activation of POMC neurons, but indicate it is not a requirement for octanoic acid-induced inhibition of neuronal activity.

### 3.7. Octanoic acid-induced regulation of POMC neuronal activity is hemichannel dependent

As GPR40 failed to influence inhibitory effects of octanoic acid on POMC neurons in the ARC, additional signaling pathways and mechanisms were explored. We first investigated whether the effects of octanoic acid were indirect and mediated through neurotransmitter-receptor signaling pathways that required activity-dependent synaptic transmission. Thus, we tested the effects of octanoic acid in the presence of the sodium channel blocker tetrodotoxin (TTX) to block activity-dependent synaptic inputs. Octanoic acid-induced responses persisted in the presence of TTX (Figure 8A,D), inducing excitation in 37.5% (6/16) and inhibition in 31.3% (5/16) of the POMC neurons, with 31.3% (5/16) of the POMC neurons being non-responsive to octanoic acid. These data are compatible with octanoic acid-induced responses in the absence of TTX (Figures 5A,B and 6A). Thus, in TTX, octanoic acid-induced depolarization was associated with an increase in neuronal input resistance and reversal potential around −90mV and octanoic acid-induced inhibition was associated with a decrease in neuronal input resistance and similar reversal potential, consistent with inhibition and activation of one or more potassium conductances (Figure 8B,C, E and F). These data suggest that the effects of octanoic acid on POMC neurons are independent of activity-dependent neural network activity and neurotransmitter release from nerve terminals.

Hemichannels are the conduit for the release of chemical messengers in a synapse-independent manner from non-neuronal tissue including the glia. Hence, we next tested the effects of octanoic acid in the presence of the gap junction/hemichannel blocker carbenoxolone (100 μM). In the presence of carbenoxolone, 83.3% (10/12) of the POMC neurons failed to respond to octanoic acid, with the remaining two neurons responding with a small depolarization and

 

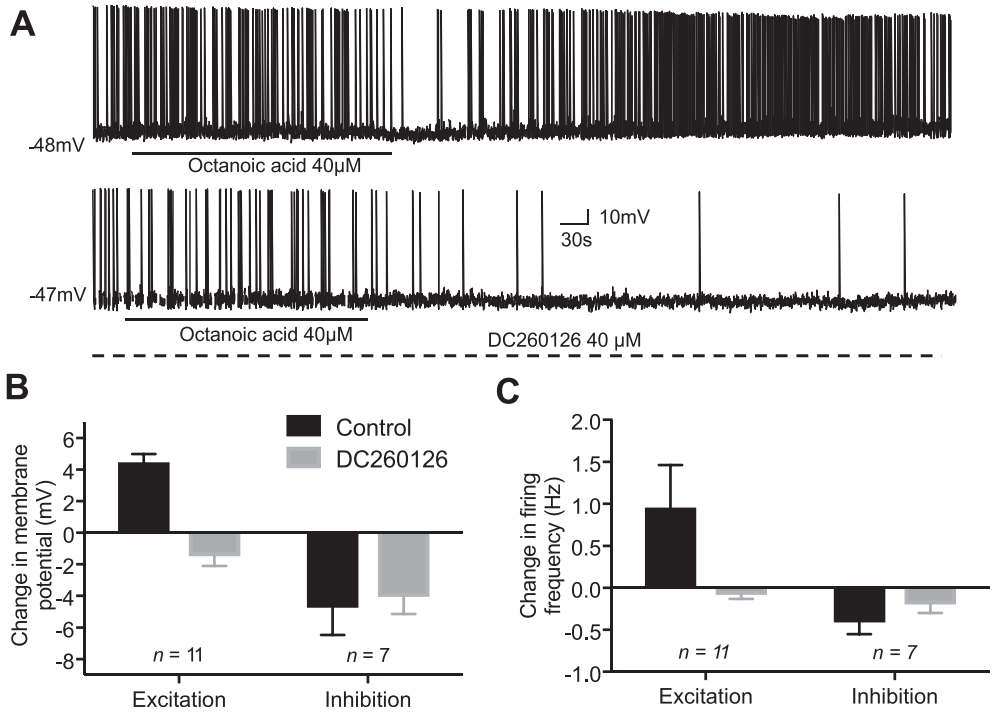


**Figure 7:** Octanoic acid-induced excitation of ARC POMC neurons via a GPR40 receptor-dependent mechanism. **(A)** Samples of a continuous whole-cell current clamp recording from an ARC POMC neuron that responded to octanoic acid with an initial transient inhibition of activity followed by depolarization and increased spontaneous activity (top trace). In the presence of the GPR40 receptor antagonist DC260126 (25 μM), octanoic acid-induced excitation was blocked, revealing a persistent inhibition of activity induced by octanoic acid (bottom trace). **(B)** Overview of effects of DC260126 on octanoic acid-induced changes in membrane potential. Octanoic acid-induced excitation was blocked in the presence of this antagonist (n = 11), revealing an octanoic acid-induced inhibition in 6 of these. DC260126 had no significant effect on octanoic acid-induced membrane potential hyperpolarization. **(C)** Overview of effects of DC260126 on octanoic acid-induced changes in spontaneous action potential firing frequency. Octanoic acid-induced increase in firing rate was blocked in the presence of this antagonist (n = 11) and had little effect on octanoic acid-induced inhibition of activity (n = 7). Data are mean ± SEM. Statistical analysis by paired two-tailed t-tests.

hyperpolarization, respectively (Figure 8G,H). These data suggest that some effects of octanoic acid are mediated via hemichannel-dependent release of a chemical messenger, which in turn regulates POMC neuronal activity. We therefore investigated the effects of antagonists of hemichannel-dependent chemical messengers such as ATP and adenosine. The adenosine $A_1$ and $A_3$ receptor antagonists DPCPX and MRS1523 had little or no effect on octanoic acid-induced inhibition of the POMC neurons (data not shown). In the presence of the $A_{2a}$R antagonist istradefylline, octanoic acid-induced membrane hyperpolarization was blocked in 5/8 of these neurons, with the response persisting in the remaining 3 neurons (Figure 9A–C). Octanoic acid-induced membrane hyperpolarization was completely blocked by the $A_{2b}$R antagonist in a further 6 POMC neurons. Taken together, these results show that octanoic acid liberates adenosine via a hemichannel-dependent mechanism and, via $A_{2a}$R and $A_{2b}$R receptors, inhibits the activity of POMC neurons.

## 4. DISCUSSION

MCFAs have been shown to improve satiation, increase energy expenditure, reduce adiposity, and promote positive health effects such as improved insulin sensitivity and glycemic control and lowering of blood lipids [18,20–22]. To date, the mechanisms underpinning these actions have remained largely unresolved. Our findings revealed the important role of MCFA octanoic acid in controlling energy balance, at least in part by regulating ARC POMC neuronal activity.

We first showed that the blood and CSF MCFA concentrations are similar and that octanoic acid constitutes the major component of MCFAs in the CSF, indicating a potential role in cellular signaling. We next showed that octanoic acid, unlike LCFA, is rapidly transported into the CNS, where it is preferentially oxidized, rather than stored, and that this is associated with rapid and transient anorexigenic actions including reduced food intake and increased energy expenditure. Furthermore, MCT administration enhanced α-MSH and neuronal activity with the PVH, indicating an engagement of the hypothalamic melanocortin system known to regulate energy homeostasis [31]. Accordingly, we investigated whether the effects of octanoic acid on energy homeostasis could be mediated by neurons within the hypothalamus that are fundamental in the control of energy balance [10,38–40]. Electrophysiological recordings within the arcuate nucleus revealed that octanoic acid altered the electrical activity of approximately two-thirds of the POMC neurons, inducing membrane depolarization and excitation or membrane hyperpolarization and inhibition of activity in subgroups of octanoic acid-sensitive POMC neurons. Pharmacological blockade of activity-dependent synaptic transmission with TTX confirmed the effects of octanoic acid on POMC neurons to be direct on the postsynaptic membrane and not mediated through neural circuit level, indirect, activity-dependent synaptic transmission. These changes in the functional operation of POMC neurons, which are fundamental to the central control of energy homeostasis, likely contributes to the anorexigenic effects and increased energy expenditure observed with octanoic acid in vivo.

 

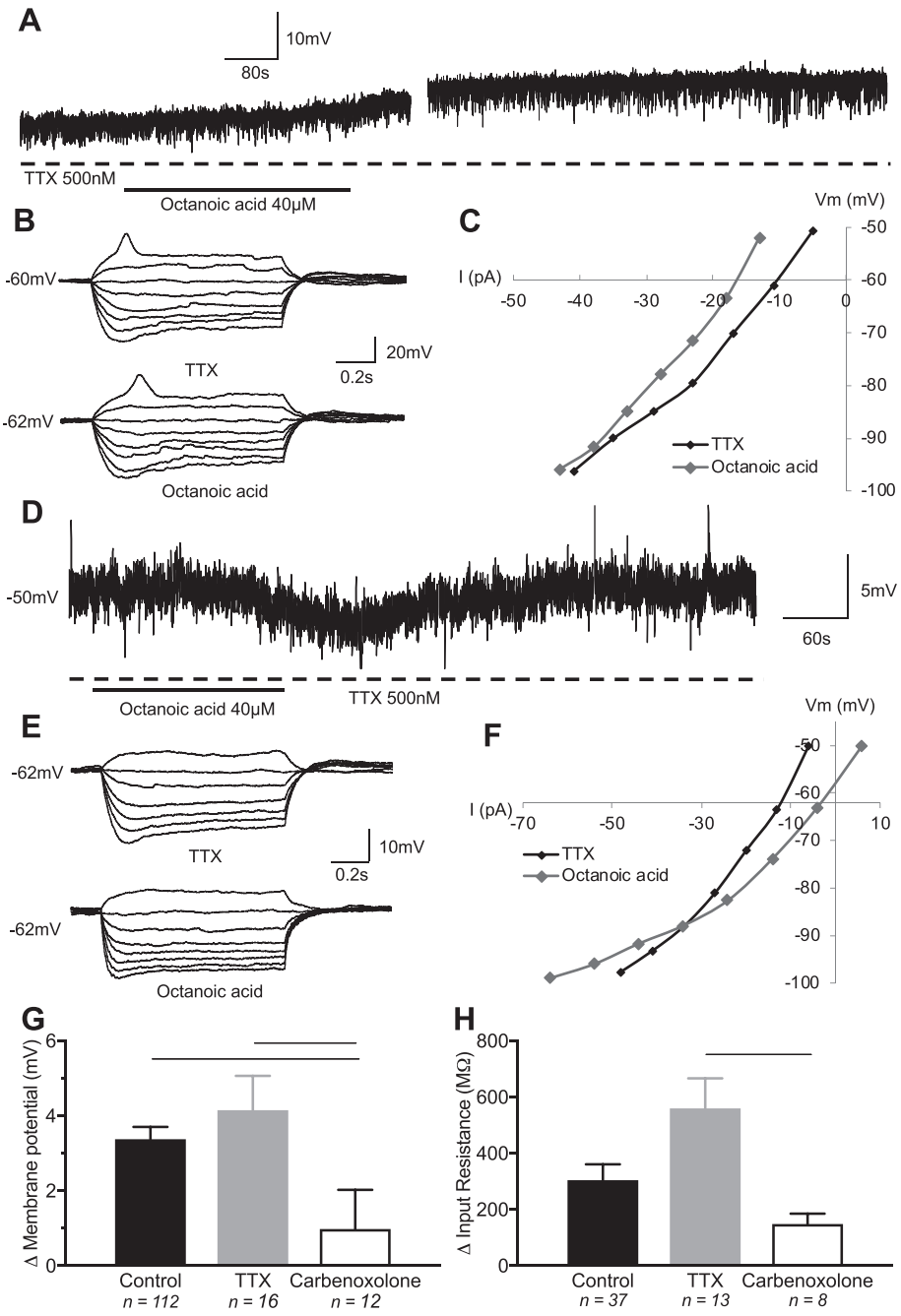


**Figure 8:** Effects of octanoic acid on POMC neurons are dependent on non-synaptic cell−cell communication. **(A).** Samples of a continuous whole-cell current clamp recording from an ARC POMC neuron showing octanoic acid-induced membrane depolarization persisted in the presence of the sodium channel blocker tetrodotoxin (TTX), indicating that the response did not require activity-dependent synaptic transmission. **(B)** IV relationships generated by injection of a linearly increasing series of negative and positive current pulses (not shown) recorded in the presence of TTX (control) and during octanoic acid-induced depolarization and TTX in an ARC POMC neuron. **(C)** Plot of IV relationships shown in B. Note the increase in the slope of the plot in the presence of octanoic acid, indicating block or inhibition of a resting conductance by octanoic acid in TTX. **(D)** Samples of a continuous whole-cell current clamp recording from an ARC POMC neuron showing octanoic acid-induced membrane hyperpolarization persisted in TTX, indicating that this response did not require activity-dependent synaptic activity. **(E)** IV relationships generated by injection of a linearly increasing series of negative and positive current pulses (not shown) recorded in the presence of TTX (control) and during octanoic acid-induced membrane hyperpolarization and TTX. **(F)** Plot of IV relationships shown in E. Note the decrease in the slope of the plot in the presence of octanoic acid, indicating activation of one or more conductances by octanoic acid in TTX. **(G)**Octanoic acid-induced changes in membrane potential were reduced in the presence of the gap junction and hemichannel blocker carbenoxolone but not by TTX. **(H)** Octanoic acid-induced changes in neuronal input resistance were reduced in the presence of the gap junction and hemichannel blocker carbenoxolone, but not TTX. Data are mean ± SEM. Data are mean ± SEM. For panels G and H, $p < 0.05$ indicated by lines adjoining bars. Statistical analysis by paired two-tailed t-tests.

 

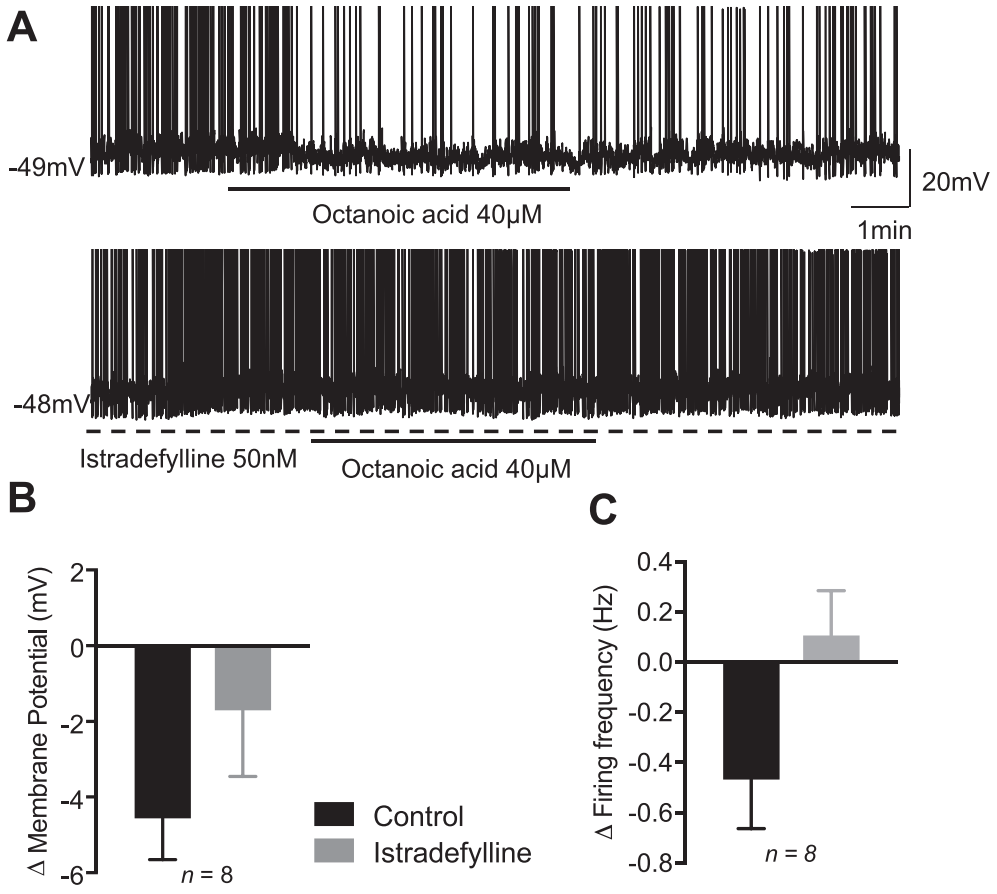


**Figure 9:** Octanoic acid-induced inhibition of ARC POMC neurons is mediated via adenosine A2a receptors. **(A)** Samples of a continuous whole-cell current clamp recording from an ARC POMC neuron showing octanoic acid-induced inhibition of spontaneous activity (top trace) and the effect that was subsequently blocked in the presence of A2 receptor antagonist istradefylline (bottom trace). **(B)** Istradefylline reduced octanoic acid-induced membrane potential hyperpolarization (n = 8). **(C)** Istradefylline reduced octanoic acid-induced firing (n = 8). Data are mean ± SEM. For panels B and C, statistical analysis by paired two-way t-tests.

Previous studies demonstrated that fatty acids can act as signaling molecules to hypothalamic neurons [13–15]. The role of long-chain fatty acids (LCFAs) as signals of nutrient availability and abundance at the level of the hypothalamic melanocortin system has been extensively studied, in particular the role of the LCFAs oleic acid and palmitic acid [41–43]. In fasted states, orexigenic NPY mRNA levels increase while the accumulation of fatty acids during the fed state suppresses NPY neurons [44,45]. Experimentally, central administration of LCFAs decrease AgRP and NPY mRNA expression and suppress food intake and glucose production [16,30,41]. These effects are most likely mediated through the entry of LCFAs into mitochondria and β oxidation. A role of carnitine palmitoyltransferase-1 (CPT1a) at the level of the CNS is also suggested, as the inhibition of CPT1a similarly decreases energy intake and glucose production [46,47]. However, overfeeding abolishes the metabolic and anorexigenic effects of centrally administered LCFAs in rodents [30]. Palmitic acid dysregulates NPY neurons, with NPY expression increasing in both whole animal and in vitro cell models [30,45] through an AMPK-dependent mechanism [43,45], inducing inflammation, endoplasmic reticulum stress, and insulin resistance [48–51].

Palmitic acid is also pro-inflammatory in POMC-expressing neurons. Palmitic acid-induced POMC synthesis is thought to occur through its uptake and metabolism, with the generation of ATP and reactive oxygen species synthesis driving these effects [52–54]. Interestingly, oleic acid can prevent, reverse, and recover the pro-inflammatory effects of palmitic acid on POMC neurons, although the mechanisms by which this is achieved are unclear [54,55]. One mechanism may be directly through changes in electrical excitability. Oleic acid has been shown to activate ATP-sensitive potassium channels [56]. In hypothalamic slice preparations, electrophysiological recordings have demonstrated that oleic acid can induce excitation of subsets of POMC neurons, but not NPY neurons, via inhibition of ATP-sensitive potassium channels [57]. The effects of oleic acid persisted in high-fat diet fed animals despite changes in the electrical excitability of these neurons, these effects being specific, based on the fact that the MCFA octanoic acid had no effect on oleic acid-sensitive neurons. β Oxidation of oleic acid in POMC neurons and its effects on their neuronal excitability via activation of ATP-sensitive potassium channels has been proposed to underlie the anorexigenic effects of this LCFA [57]. Research by Jo et al. (2009) is the only previous study to examine the effects of octanoic acid and indicated no effect on ARC POMC neurons that were sensitive to oleic acid [57]. Given that the data presented in the current paper clearly demonstrates the differential sensitivity of ARC POMC neurons to octanoic acid, including some POMC neurons that are insensitive to this MCFA, the relatively small number of

 

cells tested by Jo et al. [57], differences in recording, and mouse metabolic status (fed vs high-fat diet fed) or stage of development [58] may explain these differences.

POMC neurons have been demonstrated to be both functionally and anatomically heterogeneous [5,59–61]. Subpopulations of POMC neurons have been shown to differentially respond to leptin, insulin, and serotonin [33,59,60] and exhibit plasticity in their functional heterogeneity in response to glucose and insulin dependent upon metabolic status [35,62]. As such, the differential responsivity of POMC neurons to octanoic acid likely reflects the ability of these neurons to integrate multiple hormonal cues influencing diverse homeostatic processes.

Free fatty acid receptors are known to act as nutrient sensors and contribute to the maintenance of energy homeostasis in various regions throughout the body [63]. Previous attempts to understand how fatty acids influence the central control of energy homeostasis have focused on the transport of fatty acids into cells by fatty acid translocase (FAT/CD36) and intracellular metabolism of fatty acids, leading to the closure of ATP-sensitive potassium channels ($K_{ATP}$) [15,57,64]. Free fatty acid receptor 1 (FFA1 or GPR40) is activated by medium-to long-chain fatty acids including octanoic acid [65], is expressed within the hypothalamus, and co-localizes with POMC neurons [23,66], and activation of these receptors increases c-Fos expression in these neurons [23], the latter a marker for neuronal activation. We therefore considered GPR40 as a possible mechanism mediating the effects of octanoic acid. Pharmacological antagonism of GRP40 blocked the vast majority of the excitatory effects of octanoic acid on POMC neurons, demonstrating that octanoic acid-induced depolarization of POMC neurons was dependent on GPR40. GPR40 is a $G_{\alpha q/11}$-coupled receptor, coupled to a phospholipase C (PLC)/1,4,5-triphosphate ($IP_3$) signal transduction pathway and intracellular $Ca^{2+}$ release from intracellular stores [63,65]. Our data show octanoic acid-induced excitation of POMC neurons via GPR40 and blocking of one or more resting potassium conductances, including inwardly rectifying potassium conductances. GPR40 has previously been implicated in the development of type 2 diabetes and remains a potential drug target for treatment of this disease [63]. The data presented herein suggest GRP40 not only plays a role in regulating energy homeostasis in the periphery, but also contributes significantly at the level of the CNS; thus, future strategies targeting this receptor should take this into account.

Although GRP40 was shown to be fundamental to the octanoic acid signaling pathways driving activation of POMC neurons, it had no role in mediating the inhibitory effects of this MCFA. This study revealed octanoic acid to have a high oxidation to storage ratio, demonstrating that the majority of octanoic acid arriving within the hypothalamus undergoes β oxidation. Oxidation of fatty acids within the brain primarily occurs in astrocytes [67], which have been shown to release ATP into the extracellular space via connexin-mediated hemichannels or connexons [68,69]. Once released, ATP itself can act as a chemical messenger, or ectonucleotides in the extracellular space can rapidly convert ATP into adenosine, which in turn can also act as an extracellular signaling molecule [70,71]. Thus, we hypothesized that ATP and/or adenosine may contribute to the signaling pathway underpinning octanoic acid-induced inhibition of POMC neuronal activity. We subsequently confirmed this using selective antagonists to demonstrate a role for $A_{2A}R$ and $A_{2B}R$ in mediating octanoic acid-induced membrane hyperpolarization and inhibition of POMC neuronal activity. Furthermore, the persistence of octanoic acid-induced inhibition in TTX and suppression of the response by the hemichannel blocker carbenoxolone further supports the notion that these effects of octanoic acid are mediated by a purine-dependent signaling pathway requiring release via hemichannels rather than activity-dependent synaptic transmitter release from nerve terminals. Taken together, these effects are most likely mediated by β oxidation of octanoic acid and subsequent release of ATP from connexin/pannexin hemichannels [68,69] and subsequent conversion to adenosine, either in the extracellular space or prior to release.

Adenosine has been previously implicated in the regulation of feeding behaviors, and the role the glia play in the regulation of energy homeostasis is increasingly recognized [72,73]. Chemogenetic or optogenetic activation of astrocytes reduces food intake in normal orexigenic, and potentiates the reduction of food intake in anorexigenic situations, effects that were mediated by adenosine receptors [74,75]. Activation of the glia is associated with increased extracellular adenosine in the hypothalamus, and adenosine also reduces food intake when injected intraperitoneally [75]. Astrocyte activation leads to inhibition of AgRP neurons [74], and adenosine differentially inhibits AgRP and increases activity in POMC neurons [75]. The data presented herein suggest that octanoic acid-induced inhibition of function-specific subpopulations of POMC neurons is mediated by β oxidation of octanoic acid and release of ATP from connexin/pannexin hemichannels [68,69], with subsequent conversion to adenosine, either in the extracellular space or prior to release. Further work is required to fully clarify this signaling pathway, the source of the liberated purines, and the relative role of the glia.

In summary, this study showed for the first time how POMC neurons detect and adapt activity in response to physiologically relevant levels of MCFA octanoic acid. As a component of the melanocortin system, AgRP neurons and tanycytes form a nutrient sensing interface at the level of the blood–brain barrier. How the melanocortin neuroglial circuits integrate information regarding peripheral and central nutrient signals to formulate appropriate output and behavioral change requires further investigation.

## 5. CONCLUSIONS

In conclusion, we have identified a mechanism linking octanoic acid consumption to a rapid and transient anorectic response characterized by reduced food intake and increased energy expenditure. Once consumed, MCFAs rapidly enter the systemic circulation and traverse the blood–brain barrier, contrasting with the relatively slow entry of LCFAs into the CSF and hypothalamic parenchyma. Octanoic acid differentially modulates ARC POMC neuronal activity in two ways: directly by signaling through GPR40 and indirectly via an adenosine- and adenosine receptor-dependent mechanism. Understanding this process and the functional organization of the subsets of POMC neurons differentially regulated by octanoic acid may lead to future novel fatty acid-based therapeutic strategies to modulate energy balance.

## AUTHOR CONTRIBUTIONS

Conceived and designed the experiments: VRH, GTD, DS, MJW, and FYZ.

Conducted the experiments: VRH, NJM, MVT, FYZ, RB, GTD, DS, and DDS.

Analyzed the data: VRH, NJM, GTD, DS, and MJW.

Wrote the paper: DS, MJW, NJM, and GTD.

All of the authors edited the manuscript.

 

## ACKNOWLEDGMENTS

This study was supported by the National Health and Medical Research Council of Australia (NHMRC, ID: 1079233, 1084600, and 1063955), the Diabetes Australia Research Trust, and NeuroSolutions Ltd, UK. MJW is supported by a Senior Research Fellowship from the NHMRC (ID: 1077703). This work was supported by infrastructure and technical assistance from the Melbourne Mouse Metabolic Phenotyping Platform (MMMPP) at the University of Melbourne.

## CONFLICT OF INTEREST

None declared.

## APPENDIX A. SUPPLEMENTARY DATA

Supplementary data to this article can be found online at https://doi.org/10.1016/j.molmet.2020.01.002.

## REFERENCES

[1] Schwartz, M.W., Woods, S.C., Porte, D., Seeley, R.J., Baskin, D.G., 2000. Central nervous system control of food intake. Nature 404(6778):661—671.

[2] Enriori, P.J., Evans, A.E., Sinnayah, P., Jobst, E.E., Tonelli-Lemos, L., Billes, S.K., et al., 2007. Diet-induced obesity causes severe but reversable leptin resistance in arcuate melanocortin neurons. Cell Metabolism 5(3):181—194.

[3] Frederich, R.C., Hamann, A., Anderson, S., Lollmann, B., Lowell, B.B., Flier, J.S., 1995. Leptin levels reflect body lipid content in mice: evidence for diet-induced resistance to leptin action. Nature Medicine 1(12):1311—1314.

[4] Cone, R.D., 2005. Anatomy and regulation of the central melanocortin system. Nature Neuroscience 8(5):571—578.

[5] Mountjoy, K.G., 2015. Pro-opiomelanocortin (POMC) neurones, POMC-derived peptides, melanocortin receptors and obesity: how understanding of this system has changed over the last decade. Journal of Neuroendocrinology 27(6):406—418.

[6] Cowley, M.A., Smart, J.L., Rubinstein, M., Cerdan, M.G., Diano, S., Horvath, T.L., et al., 2001. Leptin activates anorexigenic POMC neurons through a neural network in the arcuate nucleus. Nature 411(6836):480—484.

[7] Belgardt, B.F., Okamura, T., Bruning, J.C., 2009. Hormone and glucose signaling in POMC and AgRP neurons. The Journal of Physiology 587(Pt 22):5305—5314.

[8] Cowley, M.A., Smith, R.G., Diano, S., Tschop, M., Pronchuk, N., Grove, K.L., et al., 2003. The distribution and mechanism of action of ghrelin in the CNS demonstrates a novel hypothalamic circuit regulating energy homeostasis. Neuron 37(4):649—661.

[9] Lockie, S.H., 2013. Glucagon-like peptide-1 receptor in the brain: role in neuroendocrine control of energy metabolism and treatment target for obesity. Journal of Neuroendocrinology 25(7):597—604.

[10] Zhan, C., Zhou, J., Feng, Q., Zhang, J., Lin, S., Bao, J., et al., 2013. Acute and long-term suppression of feeding behavior by POMC neurons in the brainstem and hypothalamus, respectively. Journal of Neuroscience 33(8):3624—3632.

[11] Balthasar, N., Dalgaard, L.T., Lee, C.E., Yu, J., Funahashi, H., Williams, T., et al., 2005. Divergence of melanocortin pathways in the control of food intake and energy expenditure. Cell 123(3):493—505.

[12] Lam, T.K., Schwartz, G.J., Rossetti, L., 2005. Hypothalamic sensing of fatty acids. Nature Neuroscience 8(5):579—584.

[13] Oomura, Y., Nakamura, T., Sugimori, M., Yamada, Y., 1975. Effect of free fatty acid on the rat lateral hypothalamic neurons. Physiology & Behavior 14(4):483—486.

[14] Wang, R., Cruciani-Guglielmacci, C., Migrenne, S., Magnan, C., Cotero, E., Routh, V.H., 2006. Effects of oleic acid on distinct populations of neurons in the hypothalamic arcuate nucleus are dependent on extracellular glucose levels. Journal of Neurophysiology 95(3):1491—1498.

[15] Le Foll, C., Irani, B.G., Magnan, C., Dunn-Meynell, A.A., Levin, B.E., 2009. Characteristics and mechanisms of hypothalamic neuronal fatty acid sensing. American Journal of Physiology - Regulatory, Integrative and Comparative Physiology 297(3):R655—R664.

[16] Obici, S., Feng, Z., Morgan, K., Stein, D., Karkanias, G., Rossetti, L., 2002. Central administration of oleic acid inhibits glucose production and food intake. Diabetes 51(2):271—275.

[17] Van Wymelbeke, V., Louis-Sylvestre, J., Fantino, M., 2001. Substrate oxidation and control of food intake in men after a fat-substitute meal compared with meals supplemented with an isoenergetic load of carbohydrate, long-chain triacylglycerols, or medium-chain triacylglycerols. American Journal of Clinical Nutrition 74(5):620—630.

[18] Turner, N., Hariharan, K., TidAng, J., Frangioudakis, G., Beale, S.M., Wright, L.E., et al., 2009. Enhancement of muscle mitochondrial oxidative capacity and alterations in insulin action are lipid species dependent: potent tissue-specific effects of medium-chain fatty acids. Diabetes 58(11):2547—2554.

[19] Geng, S., Zhu, W., Xie, C., Li, X., Wu, J., Liang, Z., et al., 2016. Medium-chain triglyceride ameliorates insulin resistance and inflammation in high fat diet-induced obese mice. European Journal of Nutrition 55(3):931—940.

[20] Maher, T., Clegg, M.E., 2018. Dietary lipids with potential to affect satiety: mechanisms and evidence. Critical Reviews in Food Science and Nutrition, 1—26.

[21] Papamandjaris, A.A., MacDougall, D.E., Jones, P.J.H., 1998. Medium chain fatty acid metabolism and energy expenditure: obesity treatment implications. Life Sciences 62(14):1203—1215.

[22] St-Onge, M.P., Bosarge, A., 2008. Weight-loss diet that includes consumption of medium-chain triacylglycerol oil leads to a greater rate of weight and fat mass loss than does olive oil. American Journal of Clinical Nutrition 87(3):621—626.

[23] Nakamoto, K., Nishinaka, T., Sato, N., Mankura, M., Koyama, Y., Kasuya, F., et al., 2013. Hypothalamic GPR40 signaling activated by free long chain fatty acids suppresses CFA-induced inflammatory chronic pain. PloS One 8(12):e81563.

[24] Dragano, N.R.V., Solon, C., Ramalho, A.F., de Moura, R.F., Razolli, D.S., Christiansen, E., et al., 2017. Polyunsaturated fatty acid receptors, GPR40 and GPR120, are expressed in the hypothalamus and control energy homeostasis and inflammation. Journal of Neuroinflammation 14(1):91.

[25] Folch, J., Lees, M., Sloane Stanley, G.H., 1957. A simple method for the isolation and purification of total lipides from animal tissues. Journal of Biological Chemistry 226(1):497—509.

[26] Weir, J.B., 1949. New methods for calculating metabolic rate with special reference to protein metabolism. Journal of Physiology 109(1—2):1—9.

[27] Liu, T.W., Heden, T.D., Matthew Morris, E., Fritsche, K.L., Vieira-Potter, V.J., Thyfault, J.P., 2015. High-fat diet alters serum fatty acid profiles in obesity prone rats: implications for in vitro studies. Lipids 50(10):997—1008.

[28] McQuaid, S.E., Hodson, L., Neville, M.J., Dennis, A.L., Cheeseman, J., Humphreys, S.M., et al., 2011. Downregulation of adipose tissue fatty acid trafficking in obesity: a driver for ectopic fat deposition? Diabetes 60(1):47—55.

[29] Ni, Y., Zhao, L., Yu, H., Ma, X., Bao, Y., Rajani, C., et al., 2015. Circulating unsaturated fatty acids delineate the metabolic status of obese individuals. EBioMedicine 2(10):1513—1522.

[30] Morgan, K., Obici, S., Rossetti, L., 2004. Hypothalamic responses to long-chain fatty acids are nutritionally regulated. Journal of Biological Chemistry 279(30):31139—31148.

[31] Varela, L., Horvath, T.L., 2012. Leptin and insulin pathways in POMC and AgRP neurons that modulate energy balance and glucose homeostasis. EMBO Reports 13(12):1079—1086.

[32] Schneeberger, M., Dietrich, M.O., Sebastian, D., Imbernon, M., Castano, C., Garcia, A., et al., 2013. Mitofusin 2 in POMC neurons connects ER stress with leptin resistance and energy imbalance. Cell 155(1):172—187.

  

[33] Dodd, G.T., Decherf, S., Loh, K., Simonds, S.E., Wiede, F., Balland, E., et al., 2015. Leptin and insulin act on POMC neurons to promote the browning of white fat. Cell 160(1–2):88–104.

[34] Dodd, G.T., Lee-Young, R.S., Bruning, J.C., Tiganis, T., 2018. TCPTP regulates insulin signaling in AgRP neurons to coordinate glucose metabolism with feeding. Diabetes 67(7):1246–1257.

[35] Dodd, G.T., Michael, N.J., Lee-Young, R.S., Mangiafico, S.P., Pryor, J.T., Munder, A.C., et al., 2018. Insulin regulates POMC neuronal plasticity to control glucose metabolism. Elife 7.

[36] Claret, M., Smith, M.A., Batterham, R.L., Selman, C., Choudhury, A.I., Fryer, L.G.D., et al., 2014. AMPK is essential for energy homeostasis regulation and glucose sensing by POMC and AgRP neurons. Journal of Clinical Investigation.

[37] Newton, A.J., Hess, S., Paeger, L., Vogt, M.C., Fleming Lascano, J., Nillni, E.A., et al., 2013. AgRP innervation onto POMC neurons increases with age and is accelerated with chronic high-fat feeding in male mice. Endocrinology 154(1): 172–183.

[38] Parton, L.E., Ping Ye, C., Coppari, R., Enriori, P.J., Choi, B., Zhang, C., et al., 2007. Glucose sensing by POMC neurons regulates glucose homeostasis and is impaired in obesity. Nature 449(7159):228–232.

[39] Gropp, E., Shanabrough, M., Borok, E., Xu, A.W., Janoschek, R., Buch, T., et al., 2005. Agouti-related peptide-expressing neurons are manditory for feeding. Nature Neuroscience 8(10):1289–1291.

[40] Yaswen, L., Diehl, N., Brennan, M.B., Hochgeschwender, U., 1999. Obesity in the mouse model of pro-opiomelanocortin deficiency responds to peripheral melanocortin. Nature Medicine 5(9):1066–1070.

[41] Lam, T.K., Pocai, A., Gutierrez-Juarez, R., Obici, S., Bryan, J., Aguilar-Bryan, L., et al., 2005. Hypothalamic sensing of circulating fatty acids is required for glucose homeostasis. Nature Medicine 11(3):320–327.

[42] Lopez, M., Lelliott, C.J., Vidal-Puig, A., 2007. Hypothalamic fatty acid metabolism: a housekeeping pathway that regulates food intake. BioEssays 29(3): 248–261.

[43] Tse, E.K., Salehi, Ashkan, Clemenzi, Matthew N., Belsham, Denise D., 2018. Role of the saturated fatty acid palmitate in the interconnected hypothalamic control of energy homeostasis and biological rhythms. American Journal of Physiology - Endocrinology And Metabolism 315(2): 133–140.

[44] Dziedzic, B., Szemraj, J., Bartkowiak, J., Walczewska, A., 2007. Various dietary fats differentially change the gene expression of neuropeptides involved in body weight regulation in rats. Journal of Neuroendocrinology 19(5):364–373.

[45] Fick, L.J., Fick, Gordon H., Belsham, Denise D., 2011. Palmitate alters the rhythmic expression of molecular clock genes and orexigenic neuropeptide Y mRNA levels within immortalized, hypothalamic neurons. Biochemical and Biophysical Research Communications 413(3):414–419.

[46] Obici, S., Feng, Z., Arduini, A., Conti, R., Rossetti, L., 2003. Inhibition of hypothalamic carnitine palmitoyltransferase-1 decreases food intake and glucose production. Nature Medicine 9(6):756–761.

[47] Pocai, A., Lam, T.K., Obici, S., Gutierrez-Juarez, R., Muse, E.D., Arduini, A., et al., 2006. Restoration of hypothalamic lipid sensing normalizes energy and glucose homeostasis in overfed rats. Journal of Clinical Investigation 116(4): 1081–1091.

[48] Dalvi, P.S., Chalmers, J.A., Luo, V., Han, D.Y., Wellhauser, L., Liu, Y., et al., 2017. High fat induces acute and chronic inflammation in the hypothalamus: effect of high-fat diet, palmitate and TNF-$\alpha$ on appetite-regulating NPY neurons. International Journal of Obesity 41(1):149.

[49] Mayer, C.M., Belsham, Denise D., 2010. Palmitate attenuates insulin signaling and induces endoplasmic reticulum stress and apoptosis in hypothalamic neurons: rescue of resistance and apoptosis through adenosine 5′ monophosphate-activated protein kinase activation. Endocrinology 151(2): 576–585.

[50] Benoit, S.C., Kemp, C.J., Elias, C.F., Abplanalp, W., Herman, J.P., Migrenne, S., et al., 2009. Palmitic acid mediates hypothalamic insulin resistance by altering PKC-theta subcellular localization in rodents. Journal of Clinical Investigation 119(9):2577–2589.

[51] Milanski, M., Degasperi, G., Coope, A., Morari, J., Denis, R., Cintra, D.E., et al., 2009. Saturated fatty acids produce an inflammatory response predominantly through the activation of TLR4 signaling in hypothalamus: implications for the pathogenesis of obesity. Journal of Neuroscience 29(2):359–370.

[52] Diano, S., Liu, Z.W., Jeong, J.K., Dietrich, M.O., Ruan, H.B., Kim, E., et al., 2011. Peroxisome proliferation-associated control of reactive oxygen species sets melanocortin tone and feeding in diet-induced obesity. Nature Medicine 17(9):1121–1127.

[53] McFadden, J.W., Aja, Susan, Li, Qun, Bandaru, Veera VR., Kim, Eun-Kyoung, Haughey, Norman J., et al., 2014. Increasing fatty acid oxidation remodels the hypothalamic neurometabolome to mitigate stress and inflammation. PloS One 26(9).

[54] Tse, E.K.a.B., Denise, D., 2018. Palmitate induces neuroinflammation, ER stress, and Pomc mRNA expression in hypothalamic mHypoA-POMC/GFP neurons through novel mechanisms that are prevented by oleate. Molecular and Cellular Endocrinology 472:40–49.

[55] Kwon, O., Kim, Ki Woo, Kim, Min-Seon, 2016. Leptin signalling pathways in hypothalamic neurons. Cellular and Molecular Life Sciences 73(7):1457–1477.

[56] Dadak, S.B.C., Walker, J.M., Soutar, M.P., McCrimmon, R.J., Ashford, M.L., 2017. Oleate induces KATP channel-dependent hyperpolarization in mouse hypothalamic glucose-excited neurons without altering cellular energy charge. Neuroscience 346:29–42.

[57] Jo, Y.H., Su, Y., Gutierrez-Juarez, R., Chua Jr., S., 2009. Oleic acid directly regulates POMC neuron excitability in the hypothalamus. Journal of Neurophysiology 101(5):2305–2316.

[58] Melnick, I., Pronchuk, N., Cowley, M.A., Grove, K.L., Colmers, W.F., 2007. Developmental switch in neuropeptide Y and melanocortin effects in the paraventricular nucleus of the hypothalamus. Neuron 56(6):1103–1115.

[59] Williams, K.W., Margatho, L.O., Lee, C.E., Choi, M., Lee, S., Scott, M.M., et al., 2010. Segregation of acute leptin and insulin effects in distinct populations of arcuate proopiomelanocortin neurons. Journal of Neuroscience 30(7):2472–2479.

[60] Sohn, J.W., Xu, Y., Jones, J.E., Wickman, K., Williams, K.W., Elmquist, J.K., 2011. Serotonin 2C receptor activates a distinct population of arcuate pro-opiomelanocortin neurons via TRPC channels. Neuron 71(3):488–497.

[61] Lam, B.Y.H., Cimino, I., Polex-Wolf, J., Nicole Kohnke, S., Rimmington, D., Iyemere, V., et al., 2017. Heterogeneity of hypothalamic pro-opiomelanocortin-expressing neurons revealed by single-cell RNA sequencing. Mol Metab 6(5): 383–392.

[62] van den Top, M., Zhao, F.-Y., Pattaranit, R., Michael, N.J., Munder, A., Pryor, J.T., et al., 2017. The impact of ageing, fasting and high-fat diet on central and peripheral glucose tolerance and glucose sensing neural networks in the arcuate nucleus. Journal of Neuroendocrinology 29(e12528).

[63] Ichimura, A., Hirasawa, A., Hara, T., Tsujimoto, G., 2009. Free fatty acid receptors act as nutrient sensors to regulate energy homeostasis. Prostaglandins & Other Lipid Mediators 89(3–4):82–88.

[64] Le Foll, C., Dunn-Meynell, A., Musatov, S., Magnan, C., Levin, B.E., 2013. FAT/CD36: a major regulator of neuronal fatty acid sensing and energy homeostasis in rats and mice. Diabetes 62(8):2709–2716.

[65] Blad, C.C., Tang, C., Offermanns, S., 2012. G protein-coupled receptors for energy metabolites as new therapeutic targets. Nature Reviews. Drug Discovery 11(8):603–619.

[66] Ma, D., Tao, B., Warashina, S., Kotani, S., Lu, L., Kaplamadzhiev, D.B., et al., 2007. Expression of free fatty acid receptor GPR40 in the central nervous system of adult monkeys. Neuroscience Research 58(4):394–401.

[67] Edmond, J., Robbins, R.A., Bergstrom, J.D., Cole, R.A., de Vellis, J., 1987. Capacity for substrate utilization in oxidative metabolism by neurons,

 

astrocytes, and oligodendrocytes from developing brain in primary culture. Journal of Neuroscience Research 18(4):551—561.

[68] Nualart-Marti, A., Solsona, C., Fields, R.D., 2013. Gap junction communication in myelinating glia. Biochimica et Biophysica Acta 1828(1):69—78.

[69] Newman, E.A., 2003. Glial cell inhibition of neurons by release of ATP. Journal of Neuroscience : The Official Journal of the Society for Neuroscience 23(5): 1659—1666.

[70] Meghji, P., Pearson, J.D., Slakey, L.L., 1992. Regulation of extracellular adenosine production by ectonucleotidases of adult rat ventricular myocytes. American Journal of Physiology 263(1 Pt 2):H40—H47.

[71] Ghiringhelli, F., Bruchard, M., Chalmin, F., Rebe, C., 2012. Production of adenosine by ectonucleotidases: a key factor in tumor immunoescape. Journal of Biomedicine & Biotechnology 2012:473712.

[72] Garcia-Caceres, C., Quarta, C., Varela, L., Gao, Y., Gruber, T., Legutko, B., et al., 2016. Astrocytic insulin signaling couples brain glucose uptake with nutrient availability. Cell 166(4):867—880.

[73] Djogo, T., Robins, S.C., Schneider, S., Kryzskaya, D., Liu, X., Mingay, A., et al., 2016. Adult NG2-glia are required for median eminence-mediated leptin sensing and body weight control. Cell Metabolism 23(5):797—810.

[74] Yang, L., Qi, Y., Yang, Y., 2015. Astrocytes control food intake by inhibiting AGRP neuron activity via adenosine A1 receptors. Cell Reports 11(5):798—807.

[75] Sweeney, P., Qi, Y., Xu, Z., Yang, Y., 2016. Activation of hypothalamic astrocytes suppresses feeding without altering emotional states. Glia.

 